Chapter 3

METEORITE IMPACTS, CRATERS AND MULTI-RING BASINS

3.1 The Great Bombardment

One of the principal new results of space exploration has been the demonstration that impact cratering was endemic throughout the solar system. Whether one is contemplating the cratered face of Mercury, the traces of the bombardment surviving on Venus or the Earth, the heavily cratered highland surface of the Moon or the southern hemisphere of Mars, the battered potato-like surfaces of Phobos and Deimos, the crater-saturated surface of Callisto, or the large impact crater on Mimas, the evidence is clear that a massive flux of large objects extended throughout the solar system. Although we have no direct evidence of cratering beyond Saturn, indirect evidence such as the inclination of Uranus at 90° to the plane of the ecliptic is suggestive of massive impact. Indeed, the random inclinations of the planets with respect to the plane of the ecliptic is reasonably explained as a result of massive late collisions during accretion. The evidence from samples returned by the Apollo missions provides us with a date for the steep decline in the cratering flux at 3.8–3.9 aeons. Unless special circumstances pertain to the lunar case (which were once argued, but now appear to be increasingly unlikely in view of the widespread evidence of similar heavily cratered surfaces), a general conclusion is that the bombardment continued until about 3.8 aeons, but did not persist beyond that period. The craters provide important insights into early solar system processes. The oldest observed surfaces are saturated with craters, providing evidence of the last stages of planetary accretion. The cratering rate curves for all bodies studied so far show a general resemblance, including a very high initial flux that declines rapidly between 4 and 3.5 aeons to a value close to the presently observed cratering rate. There does not seem to be any definitive evidence for a

"spike" in the cratering rate at about 3.9 aeons, as has often been suggested for the Moon.

The terrestrial geological record begins at 3.7–3.8 aeons, tantalizingly close to the fall-off in the cratering rate. Earlier crusts may have been destroyed by the bombardment but there is no isotopic or chemical signature yet detected in the oldest rocks to suggest their presence, in contrast to the early crustal formation on the Moon.

Cratering hypotheses to explain the origin of the presently observed major features of the Earth have been suggested by many workers [1]. In general, these hypotheses have not survived detailed testing. Even the oldest terrestrial rocks occur at a period when the meteorite flux has declined to a low value, so that ringed basin-forming impacts are unlikely to have occurred at times younger than 3.8 aeons. Our greater understanding of terrestrial geology and of the origins of continents and ocean basins have rendered direct analogies with lunar highlands and maria of little value (see Sections 5.12 and 9.8). This chapter deals mainly with the macroscopic effects of cratering. The related topics of micrometeorites, microcraters, regolith formation, and soil breccias are discussed in Chapter 4 on planetary surfaces. The addition of meteoritic material to the lunar surface is also considered in that chapter, as well as in Chapter 5 on planetary crusts. The effects of cratering on lunar samples, breccia and melt rock formation are also dealt with principally in Chapter 5.

The implications of cratering history for the evolution of the highland crust are considered in Chapter 5, as well as a further discussion of the lunar cataclysm and an assessment of the age data for the highland rocks. The broader implications for planetary evolution and for the planetesimal hypothesis are discussed in Chapter 9. A list of the sizes and locations of all lunar craters mentioned in the text is given in Appendix III.

3.2 The Volcanic/Meteorite Impact Debate

The nature and origin of the great lunar craters was the subject of interest and speculation for over three centuries. The debate eventually became polarized between the volcanic and meteorite impact hypotheses. The volcanic hypothesis was championed by Dana [2], Spurr [3], Green [4], and others [5, 6]. Impact origins were defended principally by Gilbert [7], Baldwin [8] and Urey [9].

In his discussion, Gilbert [7] expended much effort on the question of why lunar craters were circular, an obvious difficulty for the impact hypothesis as it was understood at the time, in view of the fact that meteorites hit the Moon at all angles. The question was not resolved until familiarity with terrestrial explosion craters and the mechanics of impact made it clear that

circular craters result from the explosive nature of impacts at high velocities, regardless of angle of impact [10].

However, various minor categories of lunar craters show some assymmetry. These include (a) elongate craters produced by the impact of secondary ejecta at low velocities, and (b) circular craters whose ejecta blankets have missing sections (e.g., Proclus, on the western edge of Mare Crisium). This ejecta pattern has been duplicated experimentally by impacts at oblique angles [11]. An alternative explanation favors the shielding effect of fault scarps [12].

Notwithstanding these special cases, the overall evidence of an impact origin for lunar craters was clear to Gilbert [7]. The argument is an interesting example of apparent constraints due to difficulties in extrapolation from familiar terrestrial conditions which occur in many scientific fields. Later analyses by Shoemaker [10] and experimental studies [13, 14], together with excellent lunar photography and familiarity with the characteristics of terrestrial explosion craters, enabled Baldwin [15] to comment in 1965 that the "136-year-old battle is over." This view has become the consensus. The first mention of the impact theory appears to have been by von Bieberstein in 1802 [16], making the debate 163 years old in 1965, although the 1829 work by Gruithuisen [16] is usually cited as the original source.

Definitive features favoring impact rather than volcanic origins include:

(a) Ejecta blankets. Simple collapse, as in terrestrial calderas, does not produce widespread deposits of thick ejecta blanket.
(b) The rayed ejecta pattern resembles that of explosion craters produced experimentally.
(c) Fresh impact craters always display pronounced elevated rims.
(d) The depth-diameter ratios fit those of terrestrial explosion and meteoritic impact craters.
(e) The energy required to excavate the largest craters and throw out the ejecta far exceeds that available from lunar seismic or volcanic processes.
(f) The production of breccias, shock-metamorphosed material and impact-melted glasses is not observed in terrestrial volcanic craters.
(g) The shock pressures, which often exceed several hundred kilobars, are not easily accounted for in volcanic eruptions. The confining pressure of the total thickness of the continental crust is only 10 kbar. Impact events produce instantaneous pressures as much as one thousand times greater than this.

Vestiges of the volcanic hypothesis for crater origin continued to haunt the lunar scene and influenced Apollo landing site selections in the lunar highlands. By that time the proponents of highland lunar volcanism had diverted their attention from the craters themselves to the nature of the smooth plains deposits covering their floors [17]. The debate continued even

during the Apollo missions [18], a fact which has prompted this lengthy account. By now, one hopes that further discussion can be left to the historians of science. A recent summary by Pike [19] provides a fitting epitaph to the debate, in which he notes (p.17) that "Although minute details of the crater or caldera proper are discussed at great length in such comparisons, the form and extent of the overall structure are almost always ignored. The latter aspects are of critical significance. . . . Two landforms so clearly different in gross surface geometry as terrestrial calderas and main-sequence lunar craters hardly can be proved to be analogous on the basis of minor morphologic characteristics."

3.3 The Mechanism of Crater Formation

Impact formed structures range in size from 0.01 microns, recorded as tiny "zap pits" in lunar samples (Fig. 3.1), to multi-ring basins over 1000 km in diameter (Fig. 3.2). As a result of intensive study over the past 20 years, we now have an excellent understanding of the broad features of impact phenomena [20–31], although problems still remain with scaling to the larger structures.

Formation times of impact craters are very short, with absolute time scales depending on the size of the ultimate crater, which in turn, is related to

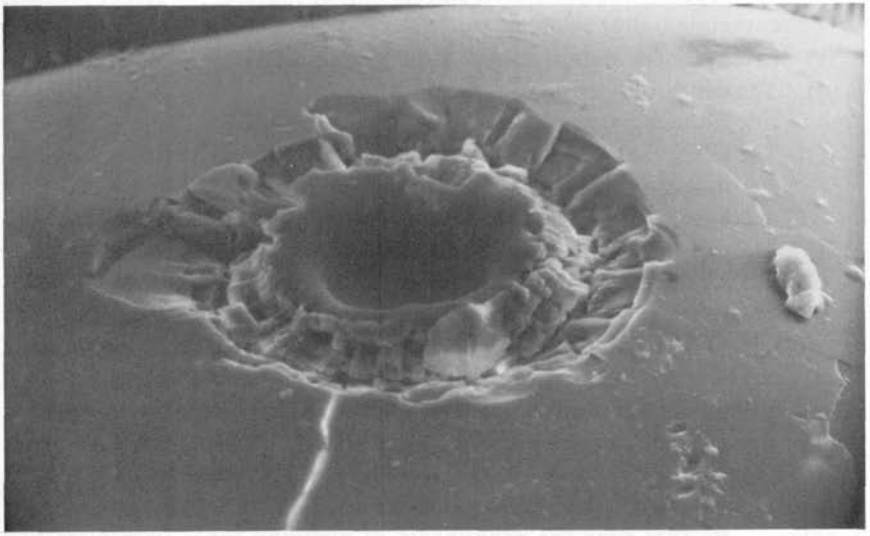

3.1 Zap pit. An SEM photo of a high velocity impact pit on a Apollo 11 glass sphere. The central pit is 30 microns in diameter. (Courtesy D. S. McKay, NASA S70-18264.)

the total kinetic energy of the impactor. Despite such short time scales, four physically distinct stages are usually recognized during the formation of a typical impact crater (Fig. 3.3):

(1) Meteorite collision, penetration and transfer of the projectile's kinetic energy into the target in the form of a shock wave.
(2) Rarefaction of this shock wave at the target's free surfaces, decompressing the volume traversed by the compressive shock wave.
(3) Acceleration of materials by the rarefaction wave and actual excavation of the crater cavity.
(4) Modification of transient crater cavity primarily due to gravitational forces and relaxation of compressed target materials.

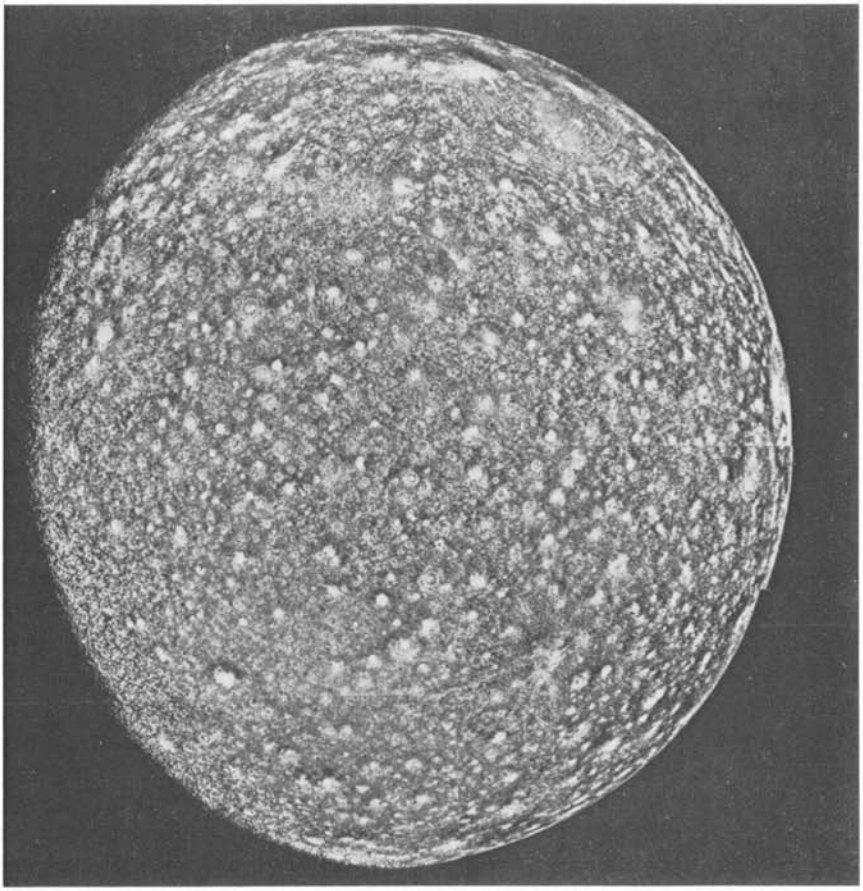

3.2 Callisto, from a distance of 390,000 km, showing the heavily cratered surface with a uniform distribution of craters. The Asgard basin is near the upper right limb.

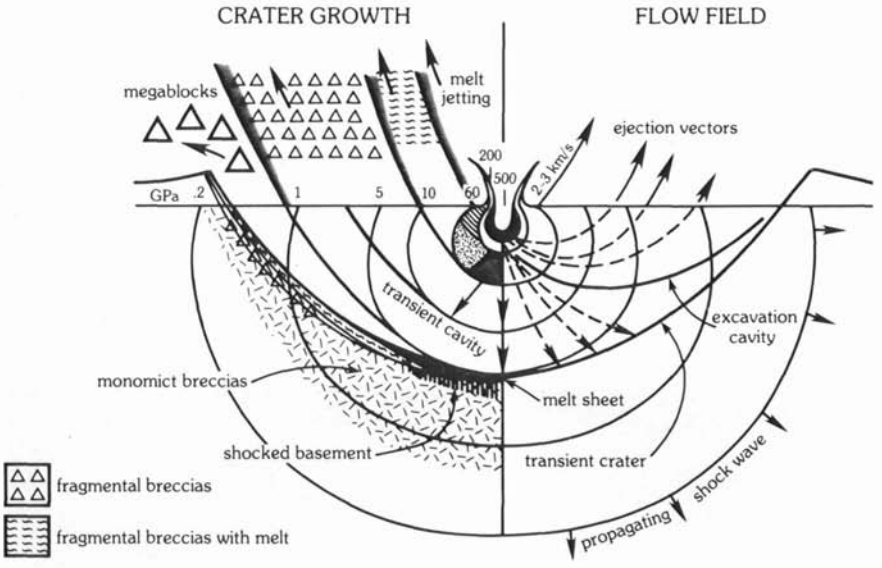

3.3 Schematic cross-section through a growing impact crater before crater modification takes place. Formation of various types of breccias are depicted on the left side. Various regimes of the melt zone are shown. Shaded lines above the target surface indicate ejecta plumes at different times. The compressed projectile is given in black. The right-hand side shows the flow field of the particle motion. The solid line defines the excavation cavity. (Courtesy D. Stöffler, *Workshop on Apollo 16.* LPI Tech. Report No. 81-01.)

Depending on crater size, phase (1) may last fractions of a second to seconds, as typical shock wave velocities are 10–13 km/sec. Phases 2 and 3 overlap in space and time and last typically 2 to 3 orders of magnitude longer, with bulk ejection velocities generally being in about the 100 m/sec range. The modification stage may last for comparable time scales. A 10-km diameter crater is thus completed within minutes, although modest gravitational adjustment may occur significantly later.

The principal energy transfer occurs via the compressive shock wave; approximately 50% is transferred into thermal energy, and 50% remains as kinetic energy in the form of ballistic crater ejecta and displacement of target materials at depth. Peak pressures in the shock wave may be 5000 kbar at cosmic impact velocities (15–25 km/sec) and sufficient to completely vaporize the projectile and some target material. Volumes engulfed by an isobar >700 kbar are generally molten. Materials that experienced 400–600 kbar may be molten in part if framework silicates are present, e.g., quartz and feldspar.

These minerals form characteristic solid-state glasses, e.g., maskelynite, at pressures between 250 and 400 kbar; rocks experiencing peak pressures < 250 kbar are mechanically deformed to variable degrees and framework silicates will display characteristic planar deformation features at pressures >100 kbar; materials subjected to < 100 kbar are typically just severely disrupted and fractured, although such phenomenon as polysynthetic twinning in, e.g., ilmenite may occur.

The total amount of melt is less than 10% of the excavated volume [31]; most of the ejecta are relatively unshocked (< 100 kbar). Although the melts have experienced the highest peak pressures, much of the melt may remain in the crater, particularly in large structures, where it accumulates in thick melt ponds and sheets [25]; this is explained by specific particle motions during the excavation stage: the highly shocked materials are predominantly driven downward into the growing cavity and the majority of the less shocked species receive a proportionally larger radial velocity component.

The rim deposits first contain unshocked material from near the surface. These are overlain by deep-seated more highly shocked materials,

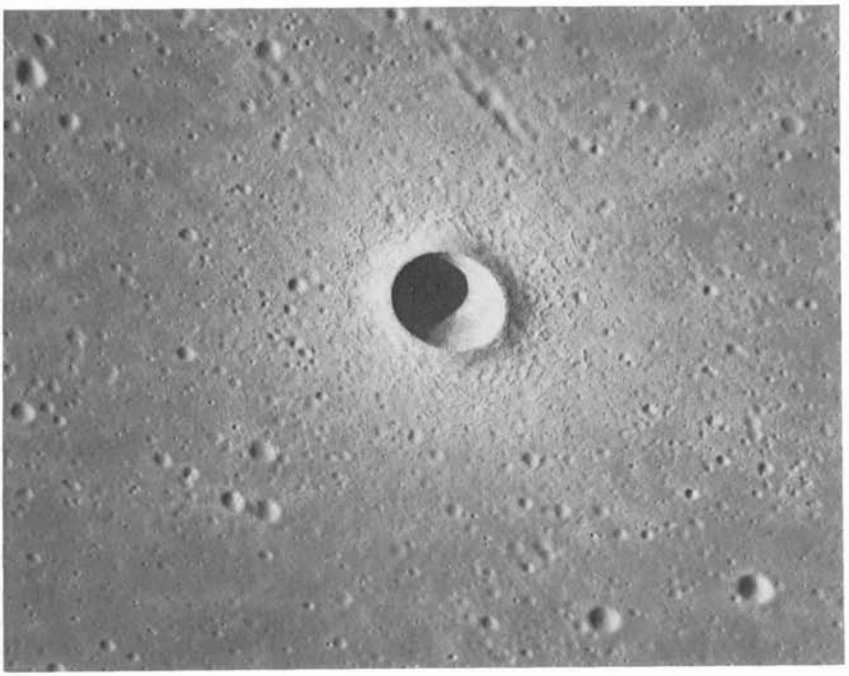

3.4 Oblique view of crater Linné in Northern Mare Serenitatis. Rim crest diameter is 2450 m. Note ejecta blocks on rim, steep walls, dune-like features on the flanks, and secondary craters at 1–3 crater radii from rim crest [19] (Apollo 15 pan photo 9353).

which produces an inverted stratigraphy. The melted material lines the sides and floor of the cavity and some flows out over the rim.

During the final modification stage, fallback of ejecta into the cavity, collapse of the walls of the transient cavity basement, rebound and uplift of the center, together with various effects due to seismic shaking, occur very quickly. Melt sheets which are draped over some of these features provide evidence that such collapses occur before the melt sheets become viscous (i.e., within a few minutes).

These models satisfactorily account for simple bowl-shaped craters, but are difficult to extrapolate to multi-ringed basin formation, just as the simple Bohr hydrogen atom model cannot be extrapolated readily to describe the structure of the uranium atom. In addition, explosion cratering on Earth may not be the best model for craters formed by meteorite impact on planets lacking atmospheres.

A fictional account of a scenario involving meteorite impacts with the Earth has been provided by Fodor and Taylor [32]. A vivid eyewitness account of an impact is given on p. 62–65 and an excellent description of a freshly formed meteorite crater (4.2 km diameter, 750 m deep, rim height 40 m above the Kansas plain), a little larger than Arizona's Meteor Crater, appears on p. 104–108. Those who wish to toil through descriptions of numerous erotic episodes will find much useful information on meteorites and on the phenomena of impact in this book.

3.4 Simple Bowl-Shaped Impact Craters

The classical example of such a crater is the Arizona Meteor Crater [33] (1100 m diameter, depth 150 m, rim height 47 m), although due to joint patterns in the bedrock the surface plan is more square than circular. One estimate for the impacting body is that it was an iron meteorite about 30 m in diameter (1.7×10^8 kg) traveling at 15 km/sec. The total energy was 1.88×10^{16} J (4.5 megaton equivalent). About 150 m of mixed breccia underlies the floor, covered by 10 m of airfall breccia. The lunar crater Linné (2450 m diameter) provides an excellent example of a fresh bowl-shaped lunar crater (Figs. 3.4, 3.5) [34].

Stratification of the target rocks, volatile content, the inherent strength of the materials and planetary gravity are the predominating factors in crater morphology. What is clear on the Earth, and to a lesser extent on the Moon and Mars, is that the form of the craters depends on the terrain. Simple bowl-shaped craters on the Moon are stable only to about 15–20 km in diameter. The major change takes place at an average diameter of 17.5 km. Eleven changes in parameters take place, marking the transitions from simple to complex craters (Figs. 3.6, 3.7). These changes are a complex function of

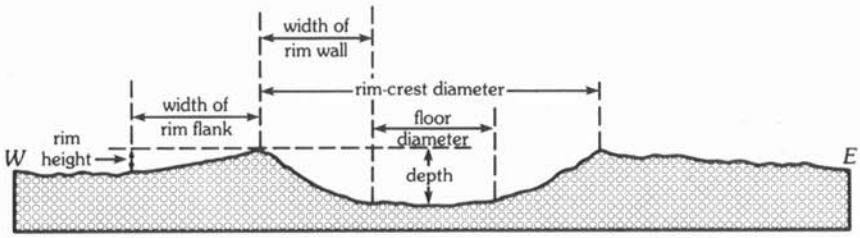

3.5 Crater terminology, illustrated by a cross-section of Proclus (28 km diameter). Adapted from [19].

the Moon's gravity, rock strength, and stresses produced by impact. Simple lunar upland craters are an average of 12% deeper than those of the same diameter on the maria. This is consistent with excavation in a deep megaregolith.

Mercury appears to have a very high target strength, stronger than that of the lunar surface. The Mercurian smooth plains and cratered terrain appear to

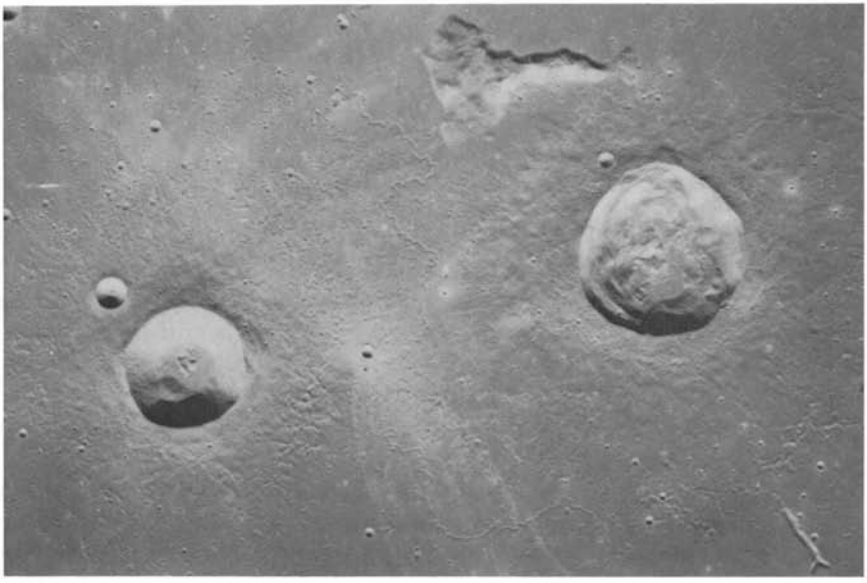

3.6 Transitions in crater morphology. The small crater at 11 o'clock from the left-hand crater is Diophantus C (5 km diameter), which resembles Linné. The adjacent 18-km diameter crater is Diophantus. The 25-km diameter crater to the right is Delisle, a complex impact crater in which slump terraces are not yet properly developed [19] (A.15 mapping camera 2738).

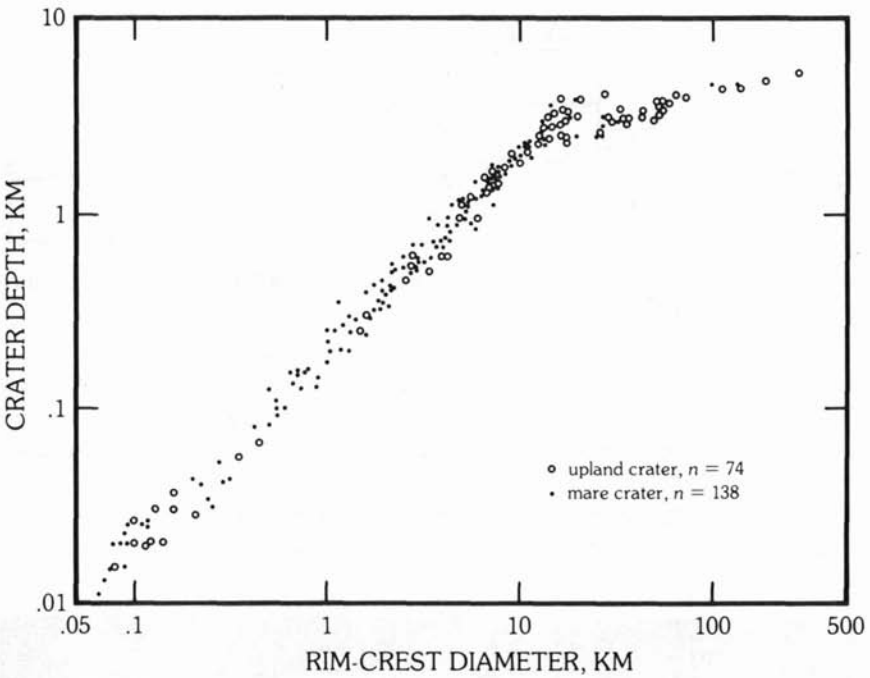

3.7 Relationship between depth and diameter for 212 fresh lunar craters (from Pike [19]). The distribution shows an inflection at about 15 km, which marks the transition from simple to complex craters on the Moon.

have the same target characteristics, suggesting that both are covered by similar material, in contrast to the difference between the lunar maria and highlands. This observation indicates the problems involved in comparing planets of differing bulk density and probably differing chemistries. However, it would be premature to use this evidence to infer that there is no megaregolith on Mercury, or that the Mercurian plains are of basaltic composition [35]. Ganymede and Callisto appear to have low target strength rocks, consistent with a water-ice crust.

The transition from simple bowl-shaped craters to complex types occurs at crater diameters of about 3 km on the Earth, about 6 km on Mars, 16 km on Mercury, and probably at 13 km on Ganymede and 15 km on Callisto. Both gravity and target characteristics appear to be involved (Fig. 3.8). Thus, simple-to-complex crater changes occur at much lower diameters in sedimentary rock than in crystalline rocks on the Earth [36, 37]. The density difference in the projectiles is also an important constraint. Iron meteorites will penetrate more deeply, whereas comet heads and carbonaceous chondrites will explode at shallower depths.

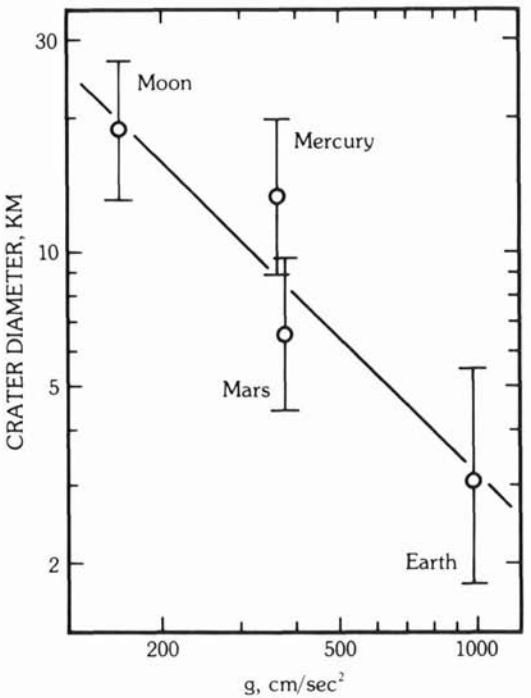

3.8 The inverse relationship between gravity and the crater diameter marking the simple to complex transition for impact craters on the Earth, Moon, Mars and Mercury. Bars are standard deviations. (Adapted from [37]. Courtesy R. J. Pike.)

The earlier concept that fresh craters in the size range 16–48 km were markedly more polygonal than smaller or larger craters [38] does not appear to be borne out by more recent data [34, p. 40]. A maximum in rim-crest circularity appears at about 10 km diameter. In comparison with mare craters, rim crests are less regular on highlands craters. The shapes of Proclus, King and Tsiolkovsky have been affected by impact into preexisting irregular topography. The rim crest relief increases rather regularly with crater diameter [34].

3.5 Large Wall-Terraced Craters, Central Peaks and Peak Rings

As noted earlier, modifications to the simple bowl shape for lunar craters begin to appear at diameters greater than about 15 km [34]. The larger craters have complex terraced walls, central peaks and flat floors. The wall terraces are well exhibited by the crater Theophilus (Figs. 3.9 and 3.10), which in addition displays a well-marked linear terrace where the crater wall has intersected the rim of the older crater, Cyrillus. Initial cavity depths may be

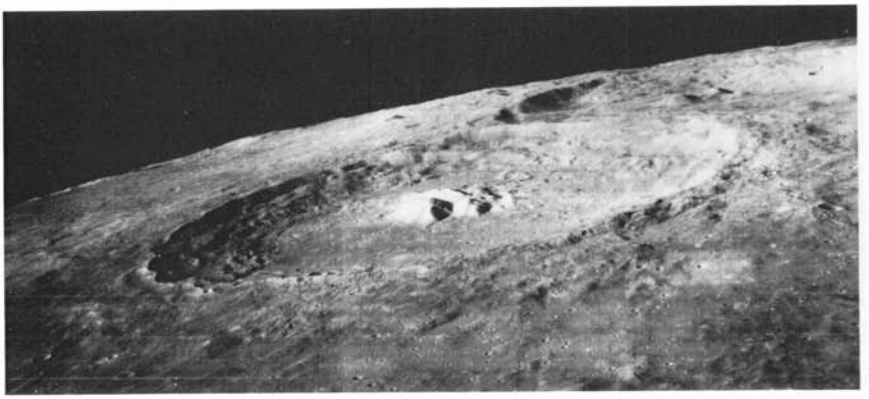

3.9 Oblique view of the lunar crater Theophilus, 100 km in diameter, showing well-developed slump terraces and a central peak complex. The straight terrace on the west wall is due to the intersection of Theophilus with the older degraded 98-km diameter crater Cyrillus (NASA Orbiter IIIM78).

estimated by restoring the slumped wall blocks to their original positions [39, 40]. The greater abundance of central peaks and wall terraces in mare craters is consistent with the greater strength of mare basalts compared to that of the highland megaregolith [34, 35]. The interest in central peaks in craters (Fig. 3.9) has been accentuated by the spectacular examples provided by the Voyager spacecraft photos of the Saturnian satellites, particularly of the 135-km diameter crater on Mimas and of others on Dione and Tethys (Fig. 3.11).

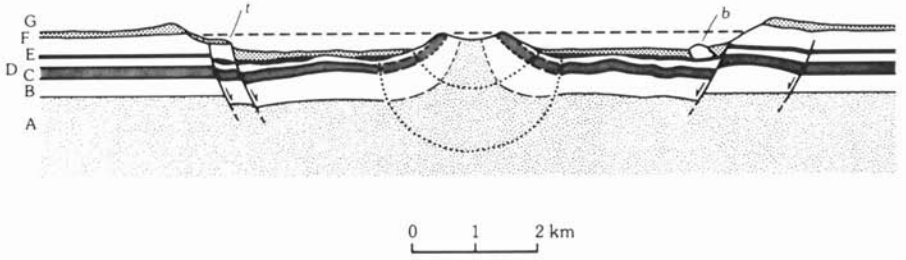

3.10 A schematic diagram of a large complex crater with slumped walls and a central peak showing uplift. The lowest unit, A, has been displaced upward by about 1 km. A and B dip vertically in the central peak. Unit G is ejecta on the crater rim, and breccia within the crater. Impact melt is not shown. The large semi-circle outlines the zone of total disruption. The smaller semi-circle marks the penetration limit of the impacting body. (Adapted from [37]. Courtesy R. J. Pike.)

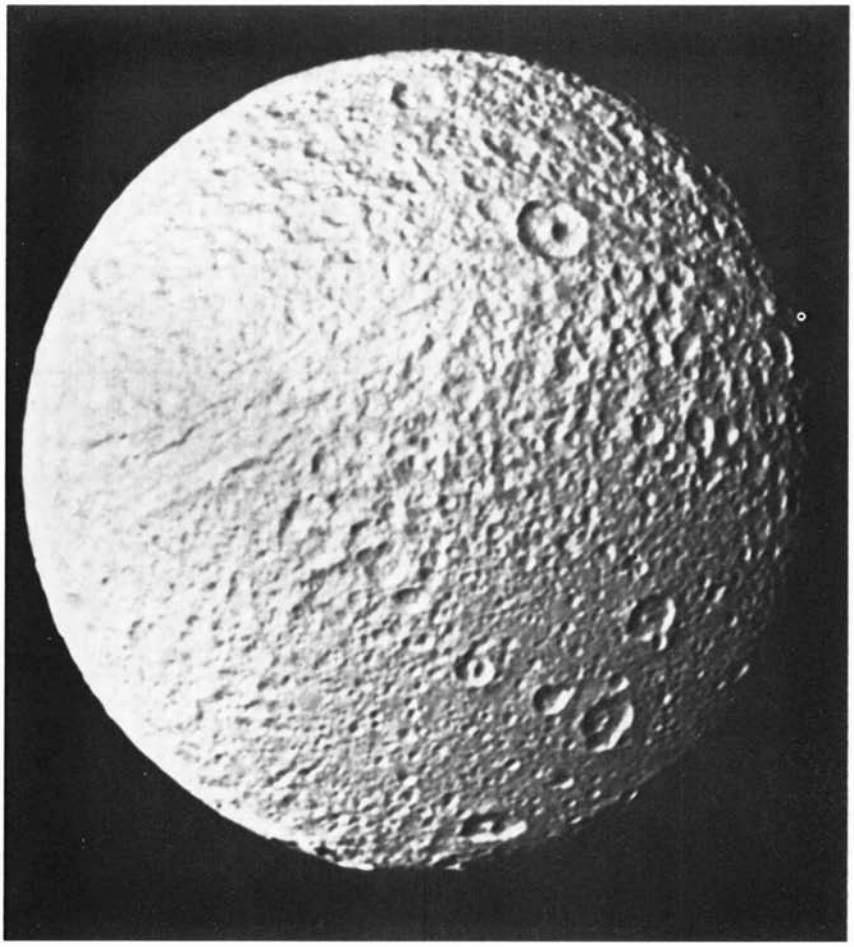

3.11 The heavily cratered surface of Tethys, showing craters down to about 5 km diameter. Note central peaks. There is a division between a heavily cratered region (top right) and a less heavily cratered area (bottom right). Tethys is 1050 km in diameter (JPL P.24065).

Central peaks appear in lunar craters at diameters greater than about 10–20 km, and all fresh lunar craters with diameters greater than 35 km have central peaks [42]. Two alternative explanations have been offered. The first is that the central peaks are thrust up by centripetal collapse of the rim [41]; the other is that they are caused by rebound. Both processes may be important [31].

The evidence from large terrestrial impact sites such as Gosses Bluff [43] and Sierra Madera, Texas [44] indicates very substantial uplift from stratigraphic horizons below those which could have been affected by rim slumping. The central peaks also seem to develop early in the cratering event [45] and so do not appear to form by isostatic readjustment (see Chapter 7). Since there is little discernible difference between craters in maria (10 m thick regolith) and highlands (2.5 km thick megaregolith), the theory that formation of central peaks requires a less cohesive surface layer overlying a more cohesive substrate must be reevaluated [46].

Although summit craters on central peaks of lunar impact craters have occasionally been reported by terrestrial observers, they are mostly illusory

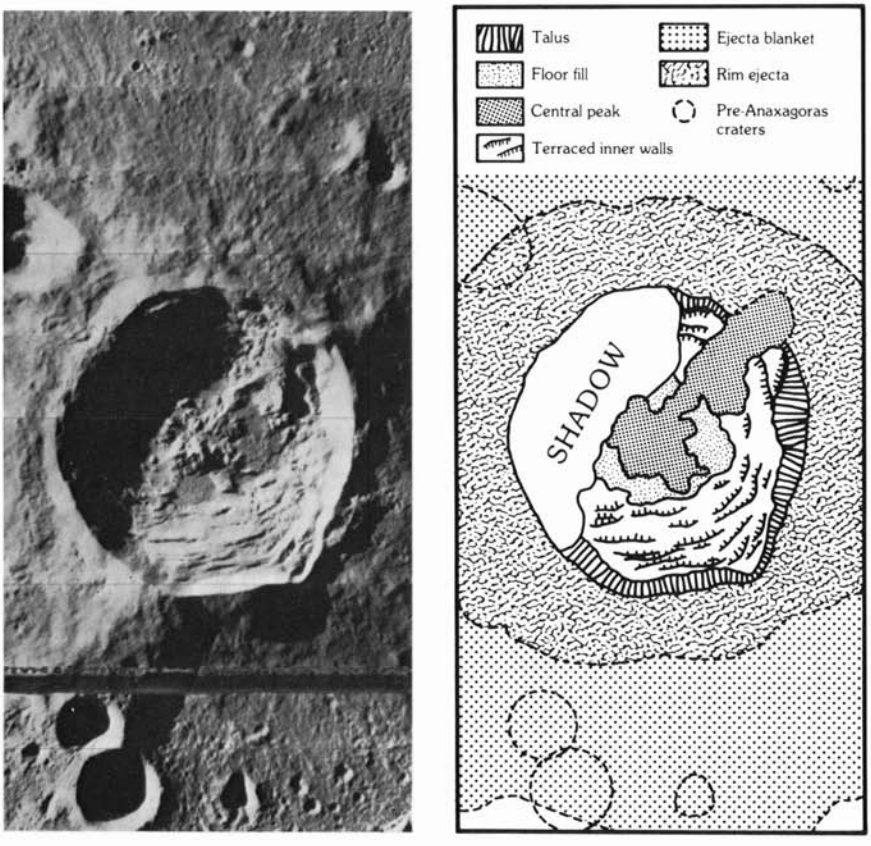

3.12 The lunar crater Anaxagoras (51 km diameter), showing an asymmetric central peak. The geological sketch map indicates that much of the central peak material overlies the terraced crater walls. The interpretation is that the central peak collapsed sideways. (Adapted from [47]. Courtesy J. B. Murray.)

3.13 The transition between central peaks and peak rings is well illustrated in this Orbiter photo (IV-8 M). The large central basin is Schrödinger (320 km diameter) which has a well-developed peak ring. The smaller crater Antoniadi (135 km diameter), at 4 o'clock from Schrödinger, has both a small central peak and a peak ring. The smaller crater just southwest of Antoniadi has a central peak only.

[34, p. 30]. A real example is the crater Regiomontanus A, a 6-km-diameter crater on the central peak of Regiomontanus (124 km diameter). It seems to be an impact crater fortuitously superimposed on the central peak. Based partly on this sort of observation, the formation of central peaks was long construed as evidence for the volcanic origin of lunar craters; however, their dissimilarity in form, compared to terrestrial volcanoes, long ago removed the analogy from serious consideration. Perhaps the most notable feature of the summit craters is their irregularity; it is rare to find symmetrical peaks. This lack of regularity constrasts with the well-developed circularity of impact craters (see [34] for details of the circularity index). The central peaks of Copernicus are well known, and show a rather jumbled topography. Other examples which show even more irregularity include Tsiolkovsky (180 km), King (77 km), Humboldt (207 km) and Anaxagoras (51 km) (Fig. 3.12).

Antoniadi (140 km) (Fig. 3.13) and Compton (165 km) represent a transitional type in that they have both central peaks and an inner peak ring. Asymmetrical ridges in Tsiolkovsky and Humboldt nearly link the central peak to the crater walls. Anaxagoras (Fig. 3.12) exhibits an extreme example of this structure, which is attributed to the sideways collapse of the central peak [47].

There is an interesting relationship between central peak size and crater diameter. The ratio of central peak diameter to crater diameter plotted as a

function of crater diameter reaches a maximum value of about 0.3 for craters of about 50 km diameter and falls off at crater diameters larger than about 70 km, although there is much scatter in the data. Peak rings occur at diameters greater than about 100 km. The central peak size decreases when rings appear, indicating a connection between the formation of central peaks and peak rings [47], which will be discussed in the next section. Maxwell [48] notes that mare wrinkle ridge rings (Section 6.16) lie too close to basin edges to represent buried peak rings. The spacing of peak rings is not the same as that of the wrinkle ridges.

The proposal that the central peak of Copernicus may be composed of olivine [49], suggested by remote-sensing data, would indicate an origin by upward movement of deep-seated material in at least two stages. The original depth of material now present in the central peak of Copernicus was about 10 km. This observation, if correct, raises interesting questions about lunar crustal structures (Chapter 5), and the nature of mascons (Chapter 7). Possibly the Copernican impact was centered on a previously uplifted mantle plug. The ultrabasic composition of the central peak of Copernicus appears to be unique: other central peaks show typical crustal signatures (Carle Pieters, pers. comm., 1981).

3.6 The Multi-Ring Basins

These are among the most spectacular landforms in the solar system, rivalled only by Olympus Mons and Vallis Marineris on Mars. Examples extend from Mercury (Caloris basin, Fig. 3.14) to Callisto (Valhalla basin, Fig. 3.15). On the Moon, 30 basins with diameters exceeding 300 km are definitely recognized, and an additional 14 are probably present (Appendix IV).

Most discussions on the origin of multi-ring basins use the superbly preserved Mare Orientale (Fig. 2.3) as the type example [50]. This basin is most clearly defined by the Montes Cordillera, which forms an impressive mountain ring with a diameter of 920 km. Typical relief is about 3 km. An inner mountain ring with a diameter of 620 km is formed by the Montes Rook. There is an Inner Rook mountain ring with a diameter of 480 km and an Inner Basin Scarp with a diameter of 320 km which borders the inner mare basalt fill (see Figs. 2.3, 3.16).

As with most multi-ring basins, there is disagreement over the location of the original crater rim. According to Head [51], the outer Rook Mountain ring (620 km in diameter) forms the rim, while the inner Cordillera ring is considered to be a fault scarp and the region between Montes Cordillera and Rook is a megaterrace. The view adopted here, for reasons given later, is that the Montes Cordillera represent the true initial rim of the Orientale basin.

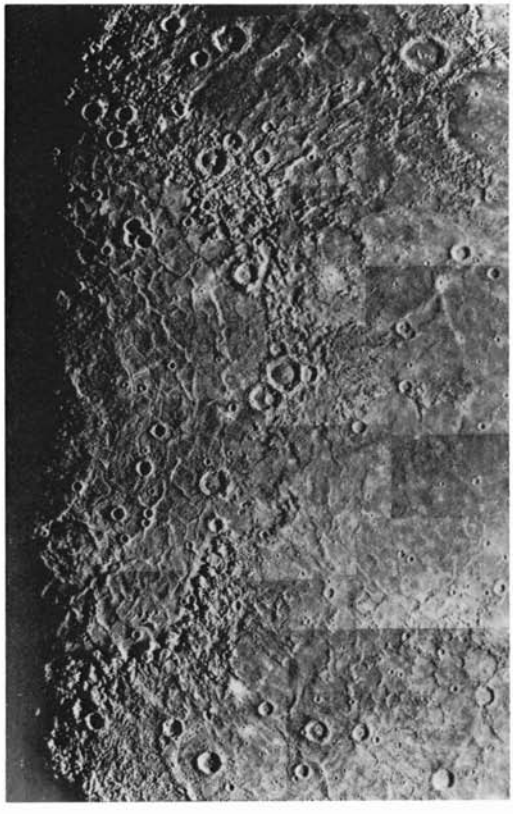

3.14 Photomosaic of Mercury, showing the Caloris basin, 1300 km in diameter, surrounded by an extensive ejecta blanket.

The deposits related to this basin are referred to as the Orientale Group and comprise the Hevelius Formation, which extends radially from the Montes Cordillera, the Montes Rook Formation, between the Cordillera and Rook Scarps, and the Maunder Formation, occupying the region between the central mare fill and the Rook Scarp. These deposits provide useful information on the origin of the basin. A significant point is that the lunar surface inside the Cordillera Scarp is very different from that outside, where a normal lunar cratered surface exists. Baldwin [52] notes that the ages of the inner basin and rings are the same, although they are much modified by the deposition of the Hevelius Formation. That is, the surface of the Orientale basin contained within the Cordillera Scarp is of the same age. A similar observation holds for the inner portion of the Nectaris basin up to the Altai Scarp. The Altai Scarp intersects the large crater Rothmann G. The portion of the crater rim inside the basin is missing. Baldwin [52] ascribes this to "fluidization," but there are many difficulties with that hypothesis. The mountain rings do not resemble frozen waves. No previous structures appear within

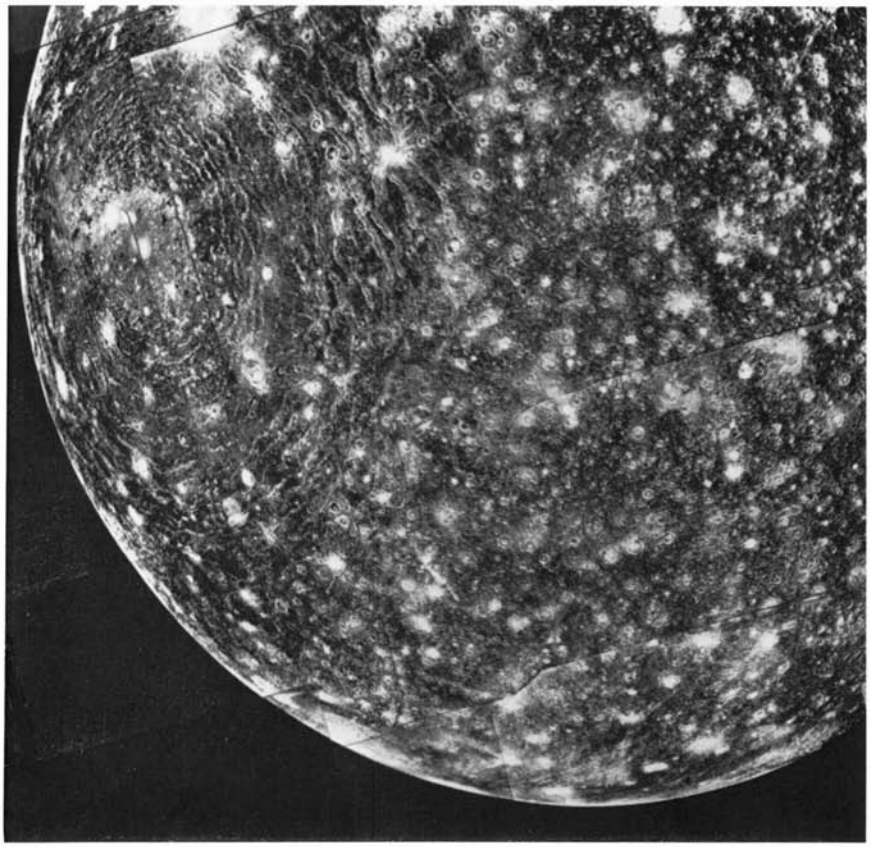

3.15 The multi-ring Valhalla basin on Callisto centered at 10° lat. 55° long.

the Apennine Mountain Ring at Imbrium, although the structure is much obscured by later mare basalt filling. The enigmatic Apennine Bench Formation (Section 2.4.4) is here interpreted as equivalent to the knobby facies of the Montes Rook Formation. Thus, it probably represents an impact melt or debris sheet ponded against the outer scarp. A controversy exists on both the diameter and depth of the original basin (Section 3.17). Here one is concerned principally with the diameter of the basin. The depth is model dependent, but the evidence appears to favor larger rather than smaller cavities. No traces of the pre-basin highland surface remain within the Cordillera, Altai or Apennine Rings.

Fault scarps circumferential to basins are occasionally observed. The most celebrated example is the set of three curved rilles, each about 2 km wide, concentric to Mare Humorum at a distance of about 250 km from the center of

that basin (Fig. 3.17). These grabens, which follow ring faults, postdate the mare fill, do not resemble megaterraces and are interpreted here as lying within the original basin rim.

Several theories of basin formation have been proposed. A principal difficulty in dealing with such phenomena is that of scale. Cratering theory can account satisfactorily for simple bowl-shaped craters up to about 1 km in diameter, but the complexities of larger craters are less readily modelled. This tends to favor notions of the hand-waving variety. In such cases, it is necessary to examine carefully all the evidence available from geological relationships to constrain hypotheses.

The most popular hypothesis has been the slumping or "megaterrace" model [51, 53–56]. Initially, a deep central bowl-shaped transient crater is formed. Later subsidence along ring faults produces the outer rings. On this

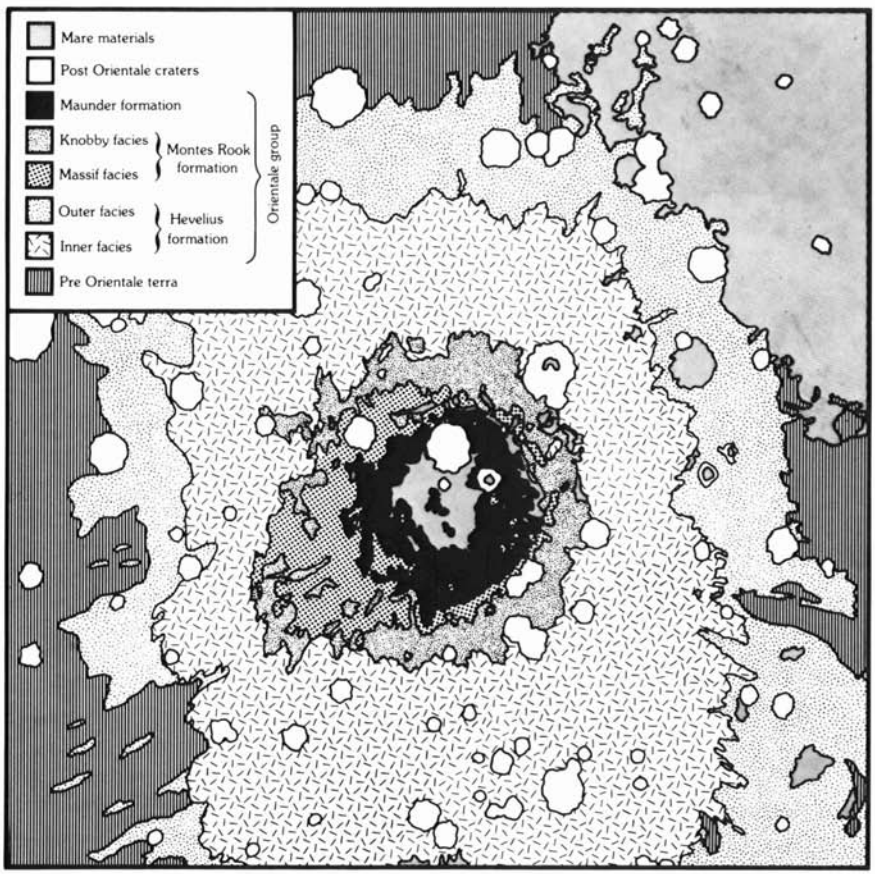

3.16 Geological sketch map of the Orientale basin.

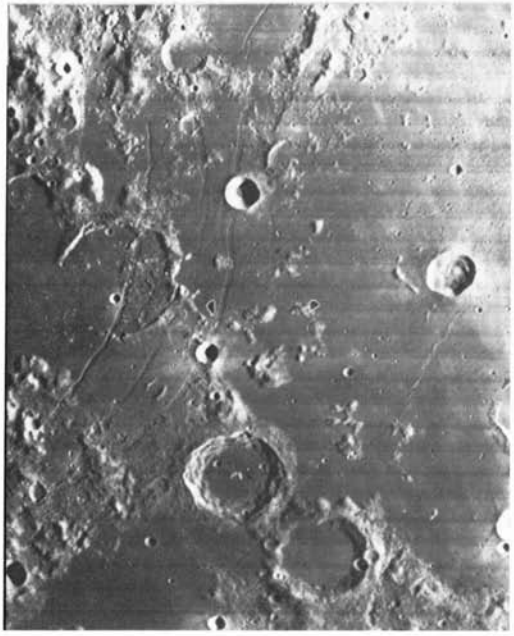

3.17 Three sets of curved rilles, about 2 km wide, concentric to Mare Humorum. The large crater, bottom right, is Campanus, 48 km diameter, flooded with mare basalt and containing a sinuous rille. The distance from the curved rilles to the center of Mare Humorum is about 250 km. The ruined crater intersected by the inner rille is Hippalus (58 km diameter) (NASA Orbiter IV-132-H).

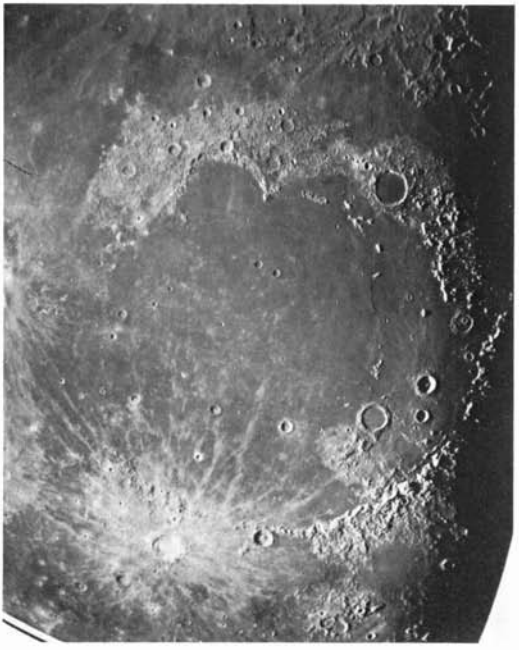

3.18 The Imbrium basin, 1500 km in diameter. Copernicus (93 km diameter) is the bright ray crater at the bottom of the picture. Sinus Iridum is the crescentic feature on the northwest rim. Plato (101 km diameter) is the flooded crater on the northeast rim. The Apollo 15 site was southeast of Archimedes, the large crater flooded with lava in the southeast quadrant inside the basin. (Rectified photo, Courtesy D. E. Wilhelms.)

hypothesis, the original diameter of Orientale is given by the Montes Rook, rather than by the Montes Cordillera. Despite the popularity of this theory, it suffers from some serious defects. The evidence favors instantaneous production of the rings during the basin-forming collision. All preexisting topography is affected out to the main outer ring. The rings are generally quite concentric, although some exceptions occur, most notably at Imbrium, where there are gaps in the outer ring and where the Montes Caucasus are not concentric with the Montes Alpes. The fact that Imbrium is not a perfect multi-ring basin [61] may be due to the formation of the basin on a topography of older multi-ring basins. Thus, it has been proposed that the Montes Alpes slid into the Imbrium basin following the impact. This model has the advantage of restoring the outer ring of Imbrium to near-circularity [61]. Probably an earlier Procellarum basin, 3200 km in diameter, occupied the area covered by the present smaller Imbrium basin [57]. It is concluded that such topographic effects can account for the irregularities observed at Imbrium. A smaller-scale example is seen on the west rim of Theophilus, where it intersects the older rim of Cyrillus (Fig. 3.9).

The "Nested Crater" model was proposed by Wilhelms et al. [58]. In this model, the rings represent the rims of concentric craters reflecting layers of differing strength in the lunar interior. Thus, for the Orientale basin, the Montes Rook ring is equated with the 25 km seismic discontinuity, while the

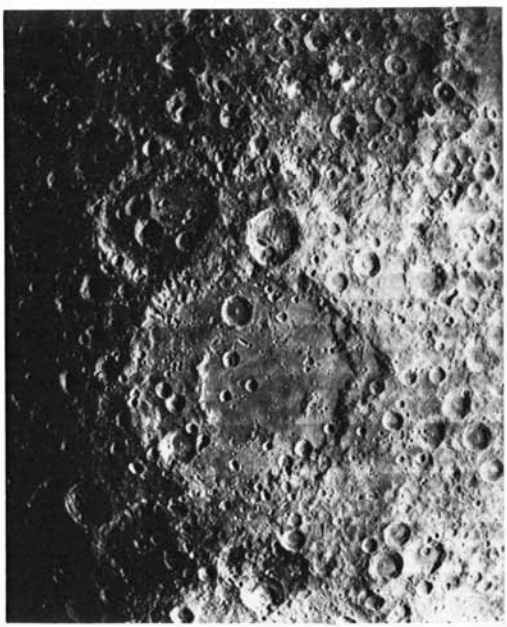

3.19 The Korolev multi-ring basin, 440 km in diameter, of Nectarian age (NASA Orbiter I 038 M).

Inner Basin Scarp represents the discontinuity at the base of the crust. The Inner Rook ring is considered to be a slumped megaterrace.

Dence [59] proposed a very deep transient crater (230 km) for Imbrium (Fig. 3.18). Instantaneous collapse into this cavity produced the outer rings. The absence of samples in the Apollo collection derived from great depths (no identifiable mantle samples have been described) makes this hypothesis less attractive, although there is evidence from the Ries crater which supports the megaterrace hypothesis. Very little material, however, is derived from deeper than 0.6 km at the Ries [31, 60].

The megaterrace model has some difficulties in explaining the regularity of the Cordillera scarp. A slumping model might be predicted to produce a much more irregular and segmented scarp than is actually observed. A particularly good example of the cratering process is provided by the Schrödinger basin (Fig. 3.13). This basin, which contains a peak ring, is about 320 km in

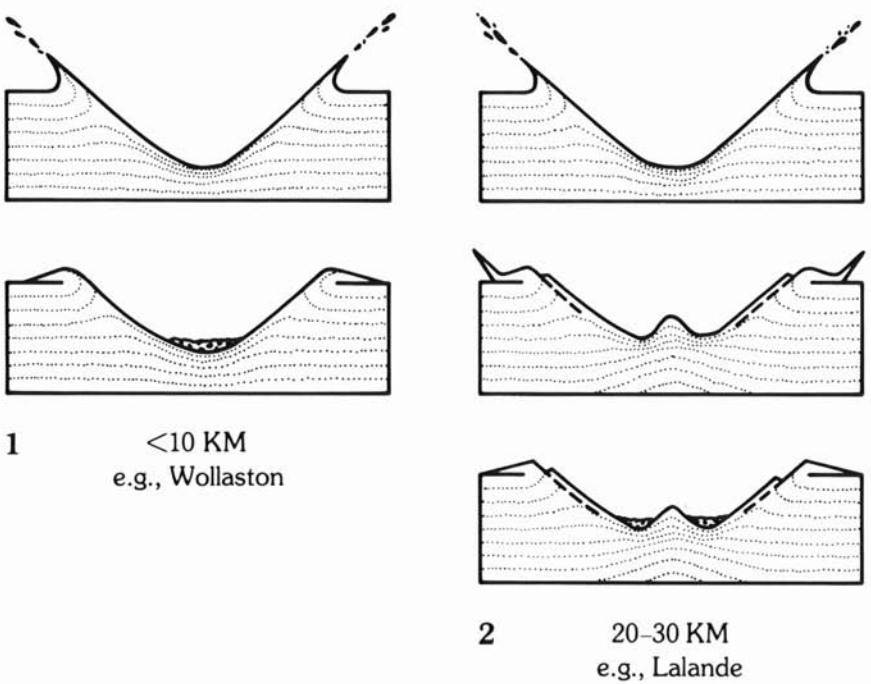

3.20 Cross-sections showing stages in the formation of impact structures in four different size ranges. The lower section in each case shows the final situation; the small circles represent crater fill. Dashed lines represent fractures. Dotted lines indicate subsurface deformation, and are not necessarily intended to represent differing layers in the substratum. See text for discussion [47]. (Courtesy J. B. Murray.)

diameter. The crater rim shows the usual terrace development as observed in Theophilus, for example (Fig. 3.9). There are no mountain rings outside the Schrödinger basin. It seems clear that the initial crater cavity for multi-ring basins must be significantly larger than Schrödinger. The ejecta blanket from Orientale is several times larger than that of Schrödinger. Accordingly, the viewpoint is taken here that the size of the initial basin is best represented by the outer mountain rings (Cordillera, Caucasus-Apennines, Altai). There does not seem to be a regular development of megaterraces as the size of the

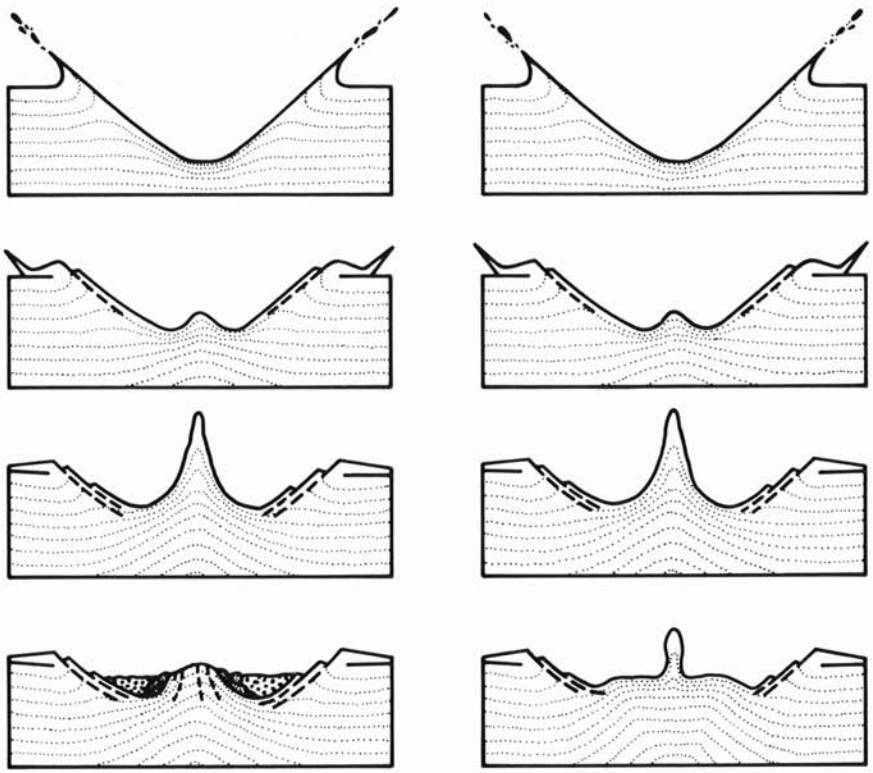

3 40–100 KM
e.g., Tycho

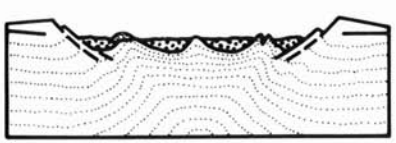

4 140–180 KM
e.g., Compton

craters increases. Thus, the small terraces at Schrödinger resemble those of Copernicus, consisting of many short irregular scarps.

Demonstrable megaterraces are not common on the Moon, although a good example exists on the western scarp of the ringed basin Korolev (Fig. 3.19). Multiple rings appear in several terrestrial craters (Ries, West Clearwater, Manicouagan, Gosses Bluff, Popigay), but evidence of fluidization appears to be lacking [62]. Other objections to the fluidization or Tidal Wave or Tsunami hypothesis include comments by Hartmann and Wood [63] that the "lunar rings do not have wave-form profiles, but rather appear to be sharply asymmetric fault scarps."

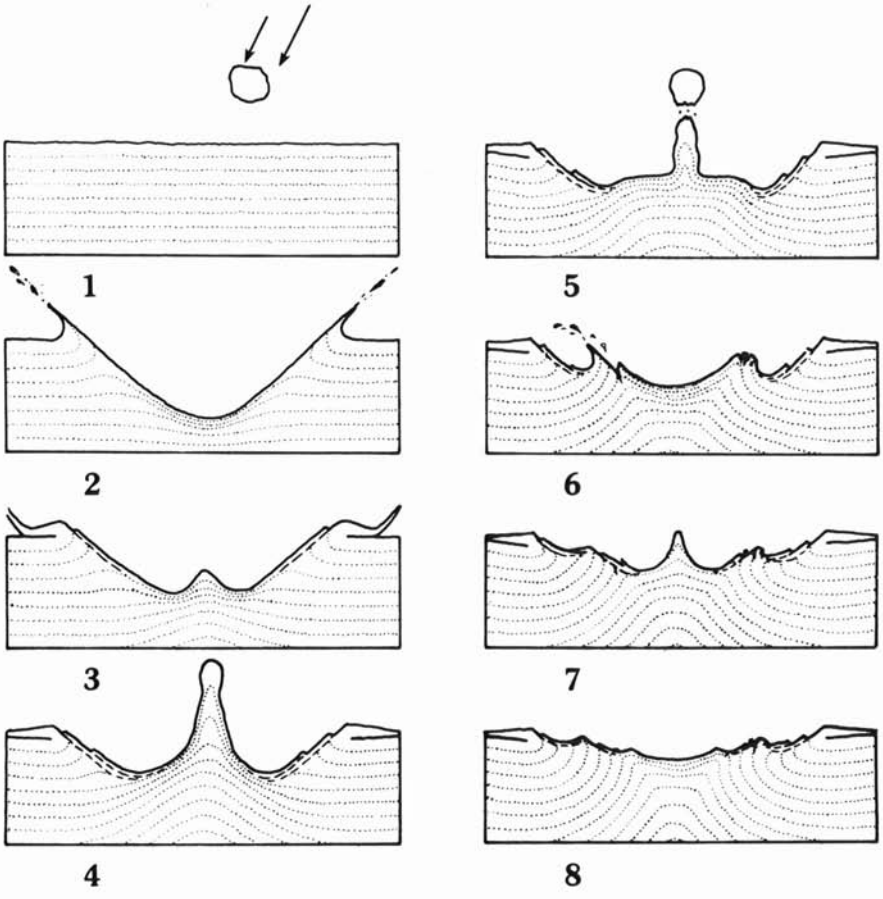

3.21 Cross-sections showing the suggested sequence of events in the formation of the Orientale basin (not to scale). See text for discussion. Symbols as in Fig. 3.20 [47]. (Courtesy J. B. Murray.)

The latest model to join the list of proposed origins for ringed basin structures is the "Oscillating Peak" model [47] (Figs. 3.20 and 3.21). The sequence of events for Orientale is as follows:

(a) The initial impact causes a bowl-shaped crater 850 km in diameter.
(b) Rebound of the center occurs, with some slumping at the crater edge and formation of terraces.
(c) Hevelius Formation is deposited. A central mound is produced. The Cordillera Scarp reaches 920 km in diameter, through terracing.
(d) Gravitational collapse of the central peak begins.
(e) Formation of an inner crater (the Montes Rook ring) occurs due to the collapse of the over-extended central peak.
(f) A second rebound occurs within the Rook crater, forming another central peak, and terracing forms the Rook Mountain ring (620 km).
(g) Collapse of the second central peak forms the Inner Rook ring (480 km) as a complex anticline.
(h) Subsequent flooding with mare basalts at a much later stage causes subsidence and formation of the Inner Basin Scarp (320 km).

Uplift of the mantle beneath the central region, together with the mare basalt fill, account for the mascon, since the mare basalt fill alone is quite inadequate to account for the positive gravity anomaly (Section 7.4.2).

Murray [47] notes that the sequence of events depends on rock behaving in a fluid fashion in very large impacts. This implies that pressures in excess of 500 kbar are involved and are experienced throughout the basin. Evidence from the lunar highland rocks does not seem to favor the development of such extensive shock pressures over the wide area of the basin.

The model draws some support from the terrestrial cratering experiments. The famous example of the Prairie Flat Crater [64, 65] formed a ringed structure in alluvium. The crater is 61 m in diameter and 5 m deep, and was formed by the explosion of a 500 ton TNT sphere. A large central peak crater (Snowball) was formed by the explosion of a hemispherical 500 ton TNT charge. Collapse of the central peak is inferred from displacement of markers, although the formation or collapse of such a peak is obscured from view during the explosion. Since this event occurred in water-saturated alluvium, conclusions may not readily be extrapolated to the Moon.

A somewhat similar model, illustrated in Fig. 3.22, incorporates features of several of the preceding hypotheses [66]. A deep parabolic central cavity forms initially. This rebounds following compression and then collapses due to gravitational forces to form a sequence of rings. A feature of the Dence and Grieve model [66], is that excavation is still occurring at the edge of the cavity, while uplift is taking place in the center (Fig. 3.22, stage b), producing a cavity which resembles a sombrero. Collapse in the rim region enlarges the cavity, reminiscent of the slumping models.

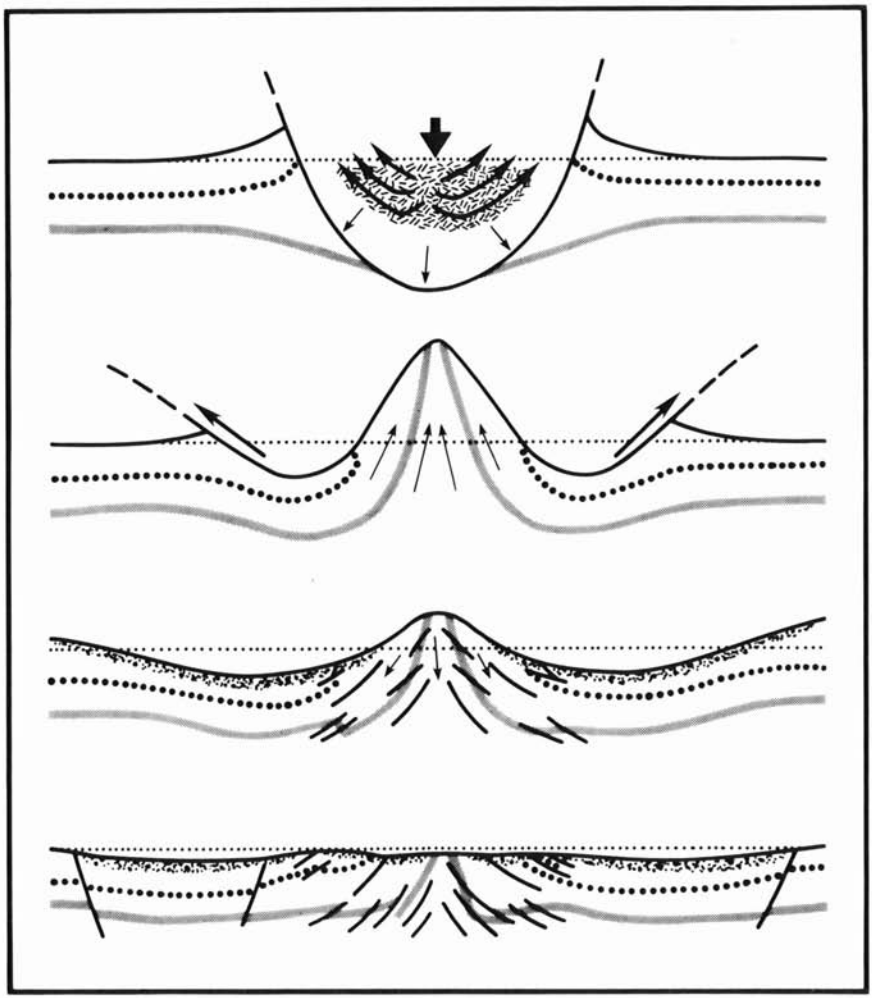

3.22 Model for the formation of ring structures. Top—formation of transient cavity by excavation and compression. Second top—rebound of compressed base of transient cavity above ground surface. Excavation from near surface at periphery is continuing. Second bottom—collapse of uplift peak under its own weight with development of reverse faulting in central area. Major excavation has ceased, although melt and breccias (stipple) are still in motion within cavity. Bottom—final configuration. Rim and uplift have reached equilibrium height controlled by rock strength and gravity. Excess volume in initial uplift, which cannot be accommodated by reverse faulting, appears as a ring. Faulting and slumping have occurred on rim. Movement of material within final crater has ceased [66]. (Courtesy R. A. F. Grieve.)

3.6.1 Very Large Basins

The distribution of lunar basins is shown in Fig. 3.23. Two very large basins occur on the Moon. Procellarum, or Gargantuan basin, has been proposed by Cadogan [57]. It is centered just to the west of the crater Timocharis at 26° N 15° W. Three rings with diameters of 1700, 2400 and 3200 km are identified, thus making this the largest impact event on the Moon. It must be older than 4.2–4.3 aeons. Like the Cheshire Cat, only the ghost of a smile or palimpsest remains of this great event.

The area south of about 45° latitude on the Moon is of unusual interest. Contained within this region are complex basins such as Schrödinger and Antoniadi (Fig. 3.13). The rima or rilles radial to Schrödinger (Rima Planck and Rima Schrödinger) are probably connected with the formation of Schrödinger basin. Antoniadi, with a central peak and a peak ring, is surrounded by an exceptionally large secondary crater field. Twelve ringed basins have been identified in the area, including the South Pole-Aitken or Big Backside basin, which is 2500 km in diameter [67].

The center of this basin is at latitude 56° S, longitude 180°. Its existence was originally postulated by Hartmann and Kuiper [68] from the observation that the Leibnitz Mountains (7–9 km high) were arcuate. Apollo laser ranging indicated the presence of a deep basin [69].

Mare Ingenii (Fig. 6.1) lies totally within this great basin, as does the crater Van de Graff. It is noteworthy that the largest negative gravity anomaly occurs within this basin. The highest concentrations of K, Th and Fe occur at Van de Graff, as well as the lowest lunar far-side concentrations of Ti. The highest magnetic anomalies likewise occur in this vicinity. The diameter of Big Backside basin is 75% of the diameter of the Moon. It can be inferred from the existence of these two giant basins that "collisional fragmentation of moon-sized bodies is difficult" [70].

The Valhalla basin on Callisto and the Caloris basin on Mercury are examples of very large basins at the inner and outer regions of the solar system (see, for example, [71, 72]) showing that cratering on this scale was ubiquitous throughout the solar system.

A tabulation of lunar basins is given in Table 3.1 and in Appendix IV.

3.7 Depth of Excavation of Basins

This is a critical question for our understanding of the composition and evolution of the lunar highland crust. Extrapolation at present from simple bowl-shaped craters to multi-ring basins clearly does not work, since this provides estimates ranging from 20–230 km [59]. Depths greater than

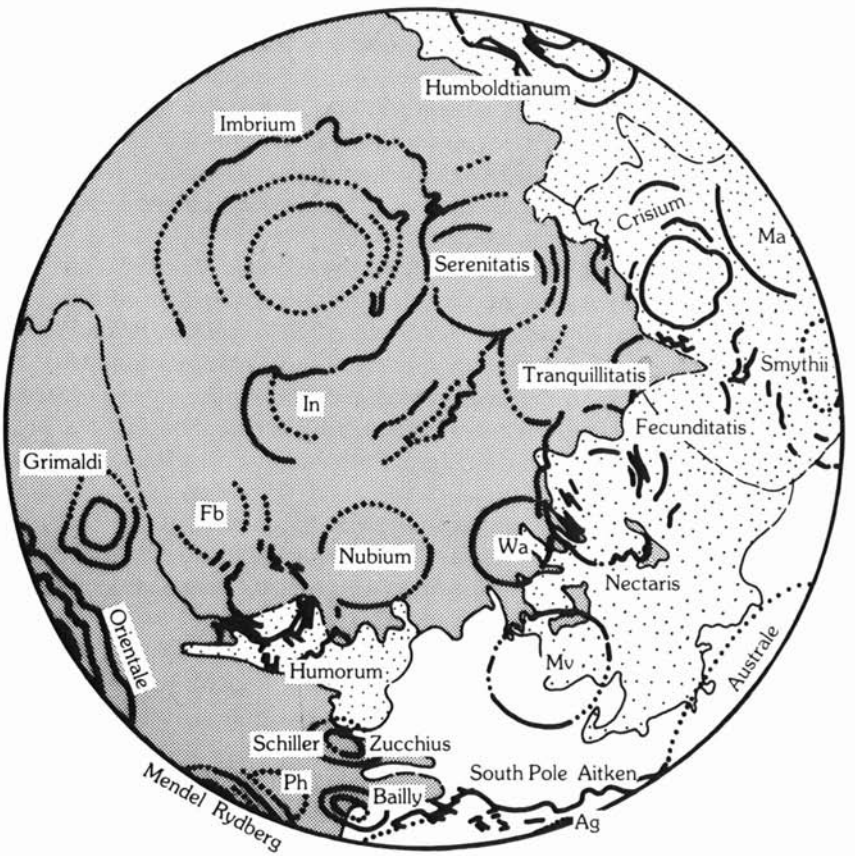

3.23 Distribution of multi-ring basins on the Moon. See Appendix IV for sizes, ages and references. Basin deposits and secondary craters have been identified around 18 basins (shown with names in capitals). (Courtesy D. E. Wilhelms.)

about 60 km are ruled out by the apparent absence of samples from beneath the lunar crust. Such samples should be readily identifiable using present models of the lunar crust, which is chemically distinct from likely mantle materials. If substantial uplift of mantle occurs during large basin formation, as is argued in Chapter 7, then mantle samples might be occasionally excavated by later impacts from shallow depths [49]. Shallow depths of excavation are possibly excluded since the depth estimates of 8–27 km [73] are less than the diameters of the impacting projectiles responsible for the excavation [27]. Estimates of 30–60 km have been made by Grieve [66] with the higher value

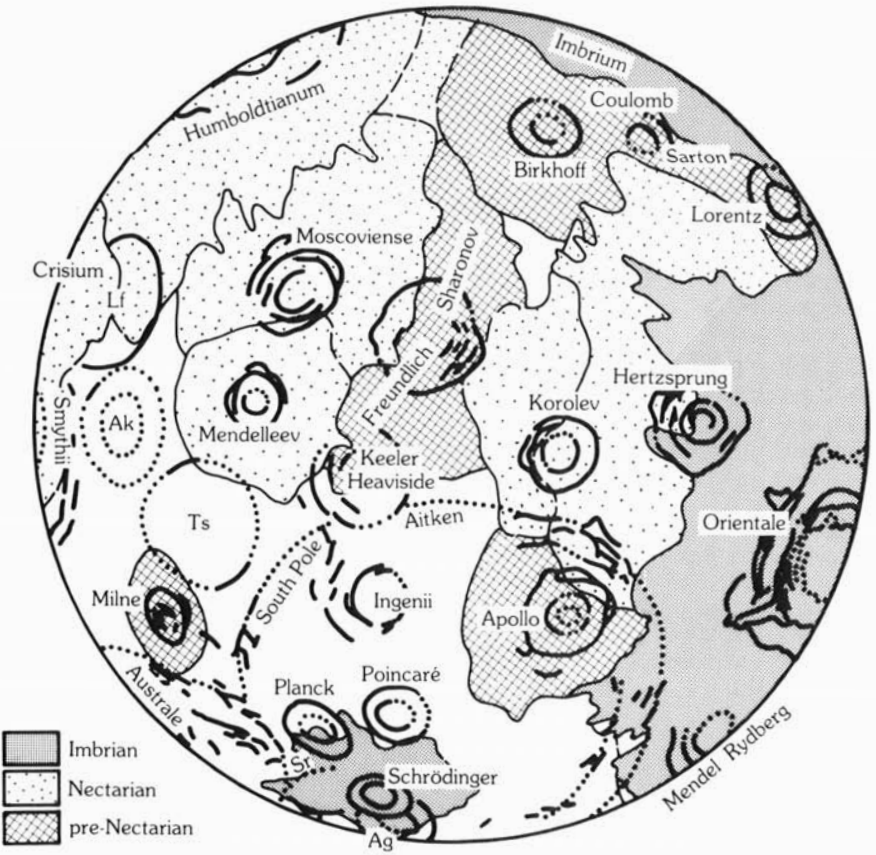

being considered more likely. Evidence of relatively deep excavation comes from the presence of spinel-bearing breccias. One ultramafic spinel cataclasite clast (15445, 177) may indeed come from the uppermost mantle of the Moon [74]. Other samples containing spinel and cordierite from Apollo 15 and 17 are identified as coming from depths of 15–32 km within the highland crust [74]. Some evidence on this question comes from the Ries crater (26 km diameter) (Fig. 3.24). Only 0.1% (wt.) of the ejecta in the continuous ejecta blanket comes from deeper than 600 m [60]. More than 99% of the Bunte breccia is unshocked and emplaced as a cool mass at ambient temperatures. Most of the thermal energy resides in the impact breccias and melts, most of which are retained within the crater structure.

These findings from the Ries crater raise questions about the interpretation of lunar samples with respect to crater ages, basin formation ages,

Table 3.1 The relative age sequence of the younger multi-ring basins, established by superposition relationships.

Source 1	Age Group	Source 2	Age Group	Source 3	Age
Orientale	IV	Orientale	2	Orientale	Imbrian
Imbrium	IV	Imbrium	3	Imbrium	
Crisium	III	Crisium	4	Crisium	
				Humorum	
Humorum	II	Humboltianum	5	Serenitatis	Nectarian†
Nectaris	II			Humboltianum	
Grimaldi	II	Grimaldi	6	Nectaris	
Serenitatis	II				
Humboltianum	II	Nectaris	7		Pre-Nectarian*
Smythii	I	Humorum	8		
Fecunditatis	I	Serenitatis	8		
Tranquillitatis	I				
Nubium	I	Smythii	9		
Australe	I				

†Additional basins of Nectarian age are: Hertzsprung, Korolev, Mendeleev and Moscoviense. Bailly is probably Nectarian.

*See Appendix for a list of 18 Pre-Nectarian basins and 11 probables.

Sources: 1. Stuart-Alexander, D. E. and Howard, K. A. (1970) *Icarus* 12: 440.
2. Baldwin, R. B. (1974) *Icarus* 23: 97.
3. Wilhelms, D. E. (1976) *PLC 7:* 2883; (1980) Multi-Ring Basins Abstracts, 115.

chemistry of basin-forming projectiles, identification of breccias with particular basins and so forth. Impact melt is mostly retained within the crater. The depth of the transient crater at Ries was about 2.5 km. If ejecta blankets are cold, not hot, then the well-documented thermal event at Apollo 14 is not related to the excavation of the Imbrium basin [60, 66, 75]! However, this problem may be resolved if a combination of shocked and unshocked, melted and cold material makes up the lunar ejecta sheets, derived from an already heavily bombarded terrain. Enough occurrences of suevite occur outside the Ries rim (Fig. 3.24) to indicate that melt escapes from the crater. The Ries is an order of magnitude smaller than the smallest lunar ringed basins, so that difficulties of extrapolation arise.

Significant progress in our understanding of excavation and sampling depths has been made since the realization that the transient crater cavity differs from the excavation cavity. Both in turn differ from the final multi-ring basin form [31]. The transient crater may be deep, and the rebound mechanism may bring up deep-seated material in the center, but most of the excavated material comes from shallower depths. The depths of excavation in the highland crust are likely to be in the range 30–60 km [23, 66]. The rebound

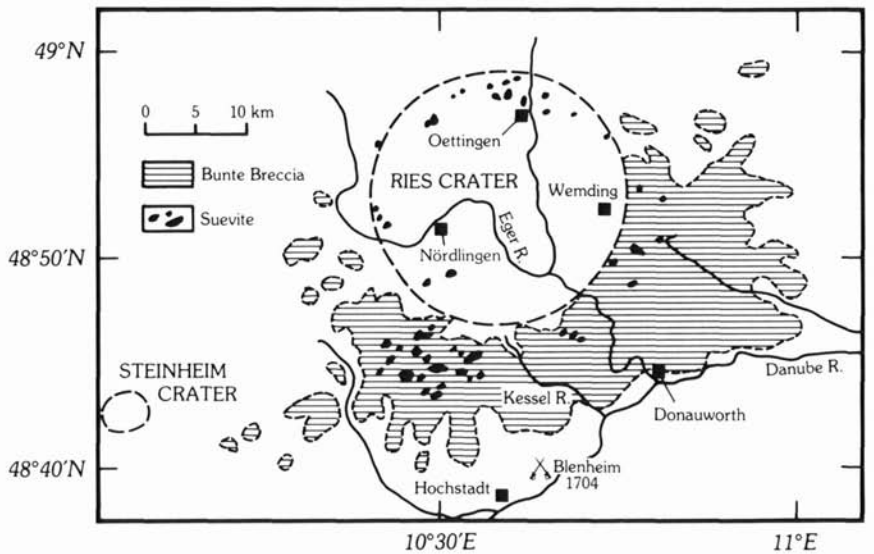

3.24 Sketch map of ejecta deposits at the Ries Crater, Germany. [After Gall, H., et al. (1977) *Geol. Bavarica* 76.]

following the production of the deep transient crater may involve a mantle plug, which does not reach the surface, but provides high density material beneath the basin. (See Section 7.4.2 on mascons.)

3.8 Basin Diameter-Morphology Relationship

Basin morphology apparently varies systematically with basin diameter on the Earth and the Moon. Thus, the sequence from simple bowl-shaped craters, to the appearance of central peaks, central peaks and peak rings (CP basins), to peak ring (PR) basins only, and then to multi-ring basins is well recognized (e.g., [76]). However, two small peak ring basins and two large central peak basins, lying outside the normal sequence, have been identified on Mars [77], so that central peak basins are not restricted to a single diameter interval and peak ring basins may occur at smaller diameters. Two large peak ring basins (Lyot and Herschel) occur at diameters on Mars where only central peak basins are observed on the Moon and Mercury.

The anomalies noted above indicate that morphology may not be simply related to diameter, but is a more complex relationship than previously realized. The new observations on the Saturnian satellites (e.g., craters on Dione and Mimas with large central peaks) must also engender caution. On

Earth, target strength (e.g., crystalline or sedimentary rock) influences the transition from simple to complex crater morphology [78] as well as on Mars [79] and Mercury [80]. In this context, peak rings within Martian and lunar basins are usually composed of short arcs or isolated peaks, but on Mercury, the rings are commonly complete.

The possibility that the "anomalous" Martian basins are caused by cometary rather than asteroidal impact is weakened by the absence of anomalous basins on other planets. The small central peak basins (50–100 km in diameter) appear to be unique to Mars. Most probably they are related to different target characteristics. The subsurface volatile layer on Mars, believed to be responsible for the fluidized craters, central peak craters, and lobate ejecta flows is often considered to be the decisive factor, but Mars is drier than the Earth.

3.9 Impact Melts and Melt Sheets

Impact melts occur commonly in and around fresh lunar craters. Most of them are retained within the crater cavity rather than being ejected. They resemble lava flows, and have been described at 55 lunar craters from 4 to 300 km diameter [81]. The melts mostly occur on crater floors and as small ponds near the crater rims; flow lobes and channels beyond the rim are prominent in

3.25 The crater Tycho (85 km in diameter) showing possible melt sheets on the crater floor (Orbiter V M 125).

craters exceeding about 10 km diameter. Flows are common in craters up to 50 km diameter.

Structures interpreted as sheets of melt-rock appear in Tycho (Fig. 3.25) and Copernicus. At Tycho, the melt sheet appears to have drained down the inner walls of the crater. At Copernicus, some apparent melt sheets have covered slumps, and slumps in other places have overridden melt sheets, indicating that the emplacement of wall slumps and melt sheets is more or less simultaneous.

Caution must be exercised in these conclusions based on photogeological interpretations. Thus, smooth deposits on the floor or Copernicus interpreted as impact melt may be fine-grained debris flows, as appears from data from the Apollo 17 infrared scanning radiometer [82]. This is another reminder of the hazards in photogeological interpretations without close ground control.

With these caveats in mind, the Apennine Bench Formation (Section 2.4.4), of uncertain origin, is here considered to be an impact melt or debris sheet from the Imbrium collision, ponded against the Apennine Mountain Scarp, which is interpreted as the edge of the Imbrium basin excavation. Thus, the Apennine Bench Formation is the equivalent in the Imbrium basin of the knobby facies in the interior of Orientale, as was noted earlier. The chemical features of melt sheets and their relationship to the parental country rock compositions is of much significance and is dealt with principally in Chapter 5 on planetary crusts.

Extrapolation of conditions from one planet to another is fraught with difficulties. On the Earth most melt sheets are derived from impacts into crystalline rocks [25]. Melts produced by impacts into sedimentary rocks are possibly finely dispersed due to expansion of volatiles. Nevertheless, even terrestrial crystalline rock terrains are probably wetter than the Martian subsurface, so that the apparent absence of "lunar-like" melt sheets on that planet cannot be ascribed to a difference in volatile contents between the Moon and Mars. A further effect is that target materials, shocked to pressures well in excess of 500 kbars, may be degassed. Repeated cratering during accretion may therefore enrich volatiles toward planetary surfaces. Cratering in the icy surfaces of the Galilean and Saturnian satellites should produce large amounts of melt and vapor, with widespread dispersal of the melt [25].

3.10 Secondary Impact Craters

These craters have caused much trouble to lunar investigators. Since they are mostly of small size, they have vitiated attempts to secure a sounder statistical base for stratigraphic ages based on crater counting; their use, which predicted very young ages for lunar maria, resulted in some loss of confidence in the simple crater counting method by the lunar science com-

munity. When crater populations are restricted to those greater than 2–4 km in diameter, then the method becomes more reliable, at least on lunar mare surfaces. A further complication is that large secondary projectiles result from multi-ring basin formation and may create secondary craters as large as 25 km in diameter.

Various characteristics may be used to distinguish primary craters. Their raised rims are about twice as high above the surrounding terrain as are those of secondaries. The rim-crest circularity is much higher for primaries: 0.81 for a sample of 44 primary craters, but only 0.57 for 29 secondaries [34]. Secondary craters also tend to be shallower, the depth-diameter ratio being 0.13 compared to 0.19 for the primary craters studied above. Herringbone or V-shaped patterns for secondaries are common and are perhaps among the most diagnostic features [83]. The tendency of secondaries to form linear crater chains has caused much confusion with possible volcanic craters. A classic example is Catena Davy (Fig. 3.26) which is a row of about 25 small craters aligned along a distance of about 48 km. These have been identified as

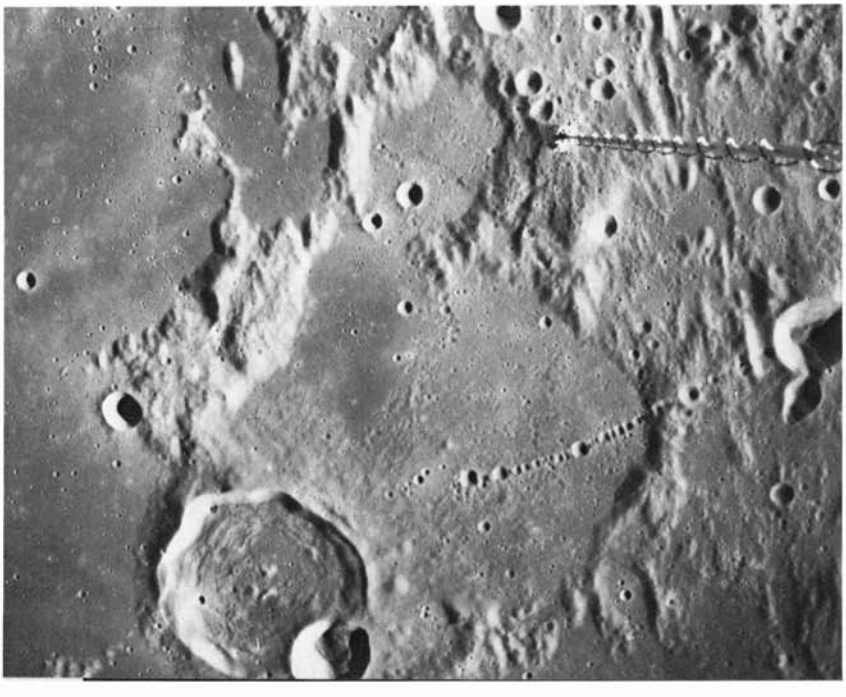

3.26 Catena Davy, a chain of some two dozen craters, formed as a result of secondary impacts, possibly from Orientale. The crater chain is 48 km long. Davy (35 km diameter) is the large complex crater in the southwest corner (AS 16-2198).

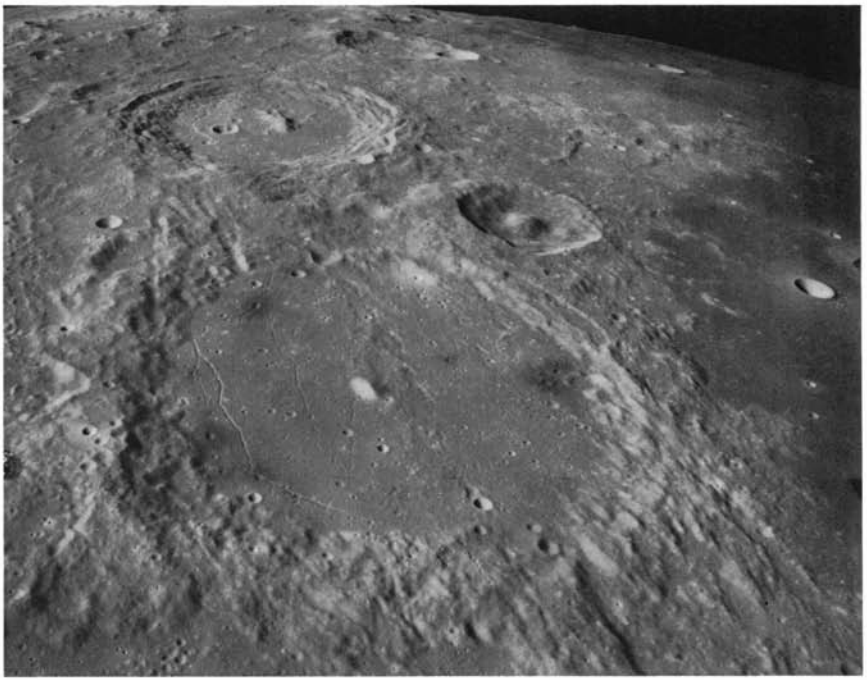

3.27 Dark halo craters, some apparently associated with rilles, on the floor of Alphonsus (119 km diameter). The large crater to the south is Arzarchel (97 km diameter). Oceanus Procellarum lies to the right (west) (AS 16-2477).

secondaries [34] and as volcanic vents but are most probably due to the former process [84]. Collapse pits along sinuous rilles add further to the complexity. The number of truly volcanic craters on the Moon appears to be small. Many dark-halo craters were originally thought to be volcanic, but are now known to be impact craters, possibly penetrating through crater ejecta into dark underlying mare basalt (e.g., Copernicus H). The dark-halo craters along the rilles in the large impact crater Alphonsus are more problematic and may be the equivalent of terrestrial cinder cones [34, Fig. 3.27]. Only a visit to them will resolve the question.

There is a wide variation in the population of secondary craters around Martian craters in the size range from 5–50 km diameter [85]. Thus, some craters (e.g., Crater Wx, 34 km diameter, in Chryse Planitia) have extensive crater fields and elongate secondaries, consistent with large ejecta, and ejection angles less than 50°. These features are consistent with impact into a competent target lithology, inferred to be basaltic lava flows [86]. In contrast, the Martian crater Arandas, 45 km in diameter [87] has very few secondaries

and the few that exist are nearly circular. These features are interpreted to be a result of meteorite impact into a low strength lithology. Experimental studies indicate high angles of ejection for such lithologies [88], which will produce circular secondary craters with near-circular rims.

Comparisons with lunar craters (e.g., Copernicus, 93 km diameter and Aristarchus, 39 km diameter) and Mercurian craters (e.g., Alencar, 110 km diameter) indicate that the secondary crater population, outside the region of continuous ejecta, is similar for the Moon and Mercury [89].

The large production of secondary craters during basin formation adds further complexity to the scene, and secondary impact by these basin ejecta has had a major modifying effect on the lunar highland landscape [90]. Basin-produced secondary craters may be very numerous even up to diameters of 25 km! This places severe restrictions on simple crater counting statistics. However, such basin secondaries may be useful stratigraphic markers, provided superposition relations among them can be recognized. The abundance of these basin secondaries further reduces the reliability of establishing a relative age sequence by crater counting unless very large areas are sampled.

Secondary craters appear to be common on the Saturnian satellites. Since they have low surface gravity and escape velocities [91] (except Titan), many secondary fragments will escape into orbits around Saturn. Most, however, will be swept up by the parent satellite. Possibly, most of the 10–20 km diameter craters on Mimas, for example, may be secondary craters [92].

When all these factors are taken into account, relative ages of planetary surfaces established by crater counting techniques have yielded remarkable insights into planetary evolution, but it is necessary to be aware of the limitations and problems with the method, as in all other dating techniques.

3.11 Dark-Halo Craters

Dark-halo craters may be either of volcanic or of impact origin. The criteria listed in Table 3.2 may be used to distinguish them [93].

Some small craters (e.g., in Alphonsus) appear to be good examples of possible volcanic craters (Fig. 3.27). They are considered to be due to explosive eruptions caused by the building of localized accumulations of volatiles. In contrast, dark-halo craters such as Copernicus H are undoubtedly of impact origin.

The questions surrounding dark-halo craters are still not properly resolved, and indicate many of the problems with the interpretation of photographs of distant objects. One recalls the difficulties in identification of common objects in close-up views (e.g., safety pins, combs, clothes pegs, etc.).

Table 3.2 Criteria for distinguishing volcanic from impact origins for lunar dark-halo craters (adapted from [93]).

Aspect	Impact Origin	Volcanic Origin
Crater shape	Circular	Often non-circular
Structural association	Random	Often aligned along rilles
Rays	Common	Absent
Ejecta deposit	Uplifted rim, dune facies, secondary craters	No raised rim, smooth ejecta blanket
Depth-diameter ratio	About 1:5 for craters less than 10 km diameter	Usually much less than for fresh impact craters

It should be noted that young craters in basaltic maria are bright, not dark. Craters of the same size adjacent to dark-halo craters frequently do not have dark haloes. There are some dark-halo craters on mare basalts. Accordingly, the conventional explanation that the dark-halo craters in the highlands represent impacts through highland debris into underlying mare basalts may not always be correct. Are the dark-halo craters caused by differences in the projectile compositions? Are they due to the impact of carbonaceous chondrites [94]? Some evidence from spectral studies has confirmed that Copernicus H has indeed excavated mare material [95]. Similar results have been obtained in regions covered by Orientale ejecta (e.g., Crater Schickard). This would indicate that basaltic volcanism was occurring before the Orientale collision, and must revise upwards our estimates of basalt volumes. Nevertheless, special caution is needed in the interpretation of dark-halo craters. Shorty crater at the Apollo 17 site, long expected to be volcanic in origin, was revealed by ground exploration to be of impact origin.

3.12 Smooth-Rimmed Craters and Floor-Fractured Craters

Several craters such as Ritter, Sabine, Lassell, Herodotus and Kopff (the latter in Mare Orientale), 20–45 km in diameter, are comparatively shallow and do not have conspicuous ejecta blankets or radial ridges. The curious case of Kopff is an often-cited example. It has been suggested that these are calderas, but they do not differ in shape from main-sequence craters of impact origin: "They simply do not have the correct shape to be calderas—and exhibit an impact crater morphology" [34]. Modification of the craters by post-impact processes seems a most promising explanation, and flooding by mare basalts seems likely in several cases [96]. This inundation produces the shallow, flat floors and buries the ejecta blankets. Janssen (23 km diameter) is

particularly unusual; its floor is 260 m above the surrounding terrain. Wargentin is another example of this rare type of crater. The most likely explanation [34] is that local hydrostatic conditions permitted flooding of the interior of the craters.

Humboldt (Fig. 3.28) and Gassendi (Fig. 3.29) are good examples of craters with bulged and cracked floors. Many other examples are known. A total of 206 such craters with pronounced floor rilles have been listed [96]. In those examples with central peaks, the peak height is usually similar to that in unmodified craters of similar diameter but the crater rim–central peak elevation difference is smaller. This suggests that relative floor uplift has occurred. Since not all craters show this effect, it cannot be due in general to isostatic uplift. Such craters are usually associated with maria (Gassendi is a prime example) so that viscous relaxation of the topography may be a viable

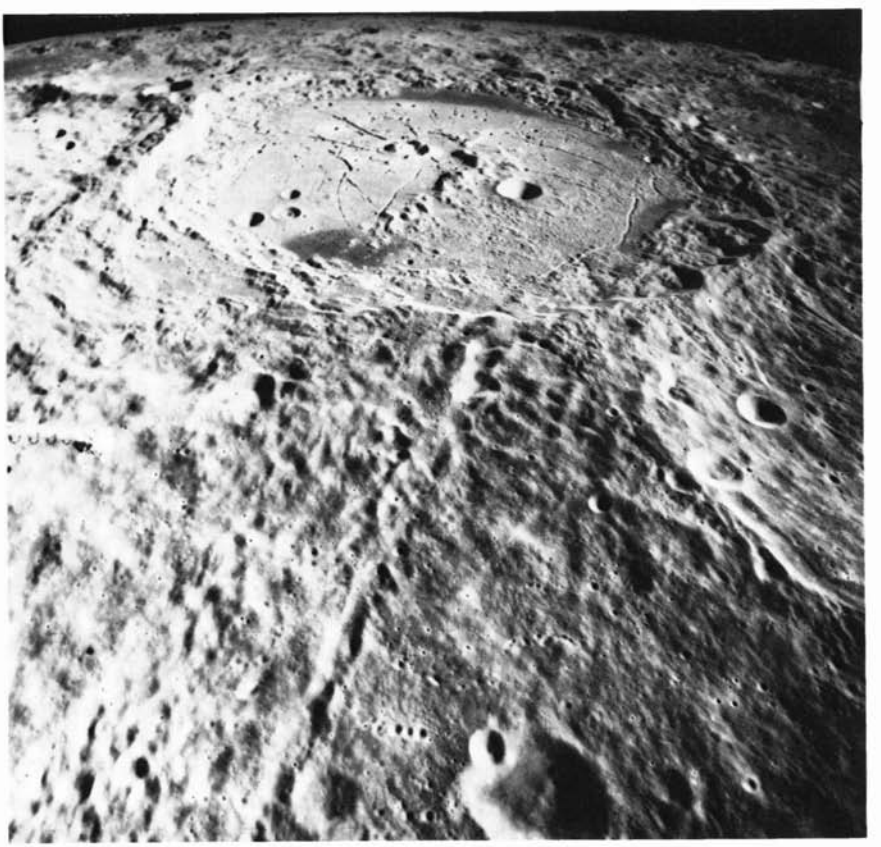

3.28 The floor-fractured crater Humboldt, 207 km in diameter (NASA AS 15-2513).

3.29 The floor-fractured crater Gassendi (110 km in diameter) (AS 16-120-19295).

mechanism in some cases [97]. The preferred explanation is that mare flooding and intrusion of sills has caused the uplift [84, 96], but the presence of similar craters on Mars and icy satellites raises further questions.

3.13 Isostatic Compensation of Craters

Isostasy probably does not affect lunar craters less than 30 km diameter [34, p. 53]. Imbrian-age craters up to about 200 km diameter (e.g., Humboldt) have zero Bouger anomalies indicating no uplift of the lunar mantle [98] and the lack of importance of large-scale isostatic processes. For fresh lunar craters, the negative Bouger anomalies (indicating mass deficiencies) can be attributed to a lens of brecciated material with a depth equivalent to about one-third the rim diameter [99]. As noted in Section 3.12, over 200 "floor-fractured" craters have been identified in which post-impact volcanic

modification has taken place resulting in apparent rise and uplift of the crater floors [84, 96, 97]. The question of isostasy and multi-ring basins, and the mascon problem, is addressed in Section 7.4.2.

3.14 Linné Crater and Transient Phenomena

Linné was initially recognized as a crater in 1823, but in 1866, Julius Schmidt reported that it had vanished and was replaced by a bright spot surrounding a 500-m-diameter crater. Various other changes were reported and Linné became the center of a controversy. The Apollo 15 mission photographed Linné, which turned out to be a very fresh normal impact crater 2450 m in diameter in western Mare Serenitatis (Fig. 3.4).

The Linné crater controversy is well described by Pike [34, p. 22]: "The detailed geometry and morphology of Linné constitute as compelling an argument for primary impact genesis as occurs anywhere on the Moon. Evidently, optical effects were responsible for the enigmatic changes in Linné, an apt testament to the perils of visual lunar observation near the resolution limit of earth-based telescopes."

3.15 Swirls

Enigmatic light-colored surface markings, named "swirls," have been observed on the far-side lunar highlands [100, 101], on the near side at Reiner Gamma [102, 103] and on Mercury [102]. They appear to have no topographic relief and cross the landscape independent of elevation. On the Moon, they are well developed in three areas: the Reiner Gamma region (5° S, 60° W), near Mare Ingenii (35° S, 180° E) and near Mare Marginis (15° N, 90° E). The origin of these swirls has been extensively debated (e.g., [102]), but they appear to be associated with impact phenomena. Preferred explanations relate them either to the antipodal effects of major basin collisions [100], or to cometary impact effects [102]. The correlation of strong surface magnetization with the Reiner Gamma feature [103] (see Section 7.8.4) lends special interest to the origin of these features.

3.16 Meteorite Flux

The latest production rate for terrestrial Phanerozoic craters with diameters greater than 20 km is about $0.36 \times 10^{-14} \text{km}^2/\text{yr}$. [104], in general agreement with previous estimates. Hartmann gave a similar estimate in 1965 [105].

This means that an impact crater with a diameter greater than 20 km will form on the Earth an average of every 30 million years.

Unless it is protected by sedimentary cover, a 20-km-diameter impact structure on the Earth has a lifetime against erosion on stable shield areas of 600 million years. A 10-km-diameter structure will survive about 300 million years, although local conditions may lead to large variations. A total of 13 terrestrial craters have associated meteoritic debris, while a further 78 structures are *probably* of impact origin, as revealed by shock metamorphic effects in the target rocks (Appendix V, Fig. 3.30). The list of these structures is increasing rapidly, and 50 additional structures are possible candidates, for which definitive evidence is currently lacking. Geochemical evidence for high levels of elements such as iridium or nickel in melt-rocks is a useful and definitive index of meteoritic impact [106, 107].

The terrestrial rate may be compared to the lunar cratering rate. The comparison must include the differences in gravitational cross-section, in impact velocities, and in surface gravity. Thus, the Earth will collect 1.24 times as many Apollo objects of the same mass per unit area as the Moon.

The estimated crater production rate for the Moon, using mare craters (with an average age of 3.4×10^9 aeons) is equivalent to a terrestrial rate of $0.37 \times 10^{-14} \text{km}^2/\text{yr}$. The two estimates are essentially in agreement. However, the mare surfaces themselves indicate that the cratering rate was still decaying at 3.4 aeons and did not become relatively constant until the period between 3.0 and 2.5 aeons. This would mean that the lunar rate between 3.0 and 2.5 aeons was lower than the observed terrestrial rate during the Phanerozoic by perhaps a factor of two. The inference is that the crater production rate has not been constant in the Earth-Moon system during the past 3 billion years, and that the Phanerozoic may have been a time of elevated crater production. This problem may be resolved by better statistics, but may indicate the true state of affairs. It would not seem unreasonable that wide fluctuations occur, and that their frequency would increase with time as more and more objects are swept up by the planets, thereby increasing the randomness of the individual events [108].

The question of whether the craters on the lunar highland surface can be interpreted as representing a saturated surface or a continuing production rate remains unsolved [66]. If the craters represent a production population, then they can be used to establish the relative ages of various surfaces in the highlands (Table 3.3), as well as the average depth of sampling, number of impacts per sample, and the volume of impact melt produced. If the cratering record represents saturation, then it provides only a minimum estimate for ages, and the integrated thermal effects will be severe. If the observed cratering record is a true account of the bombardment history back to 4.5 aeons, then there are severe discrepancies between the amount of impact melt produced and the radiometric age record [109].

Table 3.3 Estimates of ages of geologic provinces on the Moon.†

Geologic Province	Crater Density Relative to Average Lunar Mare	Estimated Crater Retention Age (aeons)			Regolith Thickness (m)
		Minimum	Best Estimate	Maximum	
Tycho	0.1	0.09	0.3	0.6	—
Aristarchus	0.2	0.5	0.9	1.3	—
Copernicus	0.3	0.8	1.5	2.2	—
Mare Crisium	0.5	2.1	2.6	3.5 ?	—
Mare Imbrium	0.50	2.2	2.6	3.5	—
Whole Mare Serenitatis	0.65	2.8	3.1	3.7	—
S. Oceanus Procellarum	0.75	3.0	3.3	3.7	3
Mare Fecunditatis	0.93	3.2	3.4	3.8	—
Average of front-side maria	1.00	3.3	3.5	3.8	5
Mare Orientale	1.10	3.3	3.5	3.8	—
Mare Tranquillitatis	1.30	3.5	3.6	3.9	5
Mare Humorum	1.50	3.6	3.7	3.9	—
Mare Nubium	2.5	3.8	3.9	4.0	—
Orientale basin and ejecta	2.5	3.8	3.9	4.0	—
Fra Mauro	3.0	3.9	4.0	4.1	8
Fill in Schrödinger basin	5.1	4.0	4.1	4.2	—
Fill in Mendeleev crater	9	4.1	4.2	4.2	—
Front-side highlands	10	4.1	4.2	4.2	10–15
Heavily cratered highlands and basins	32	4.3	4.4	4.5	megaregolith
"Pure" highlands	36	4.3	4.4	4.5	megaregolith

†Adapted from *Basaltic Volcanism* (1981) Table 8.6.1.

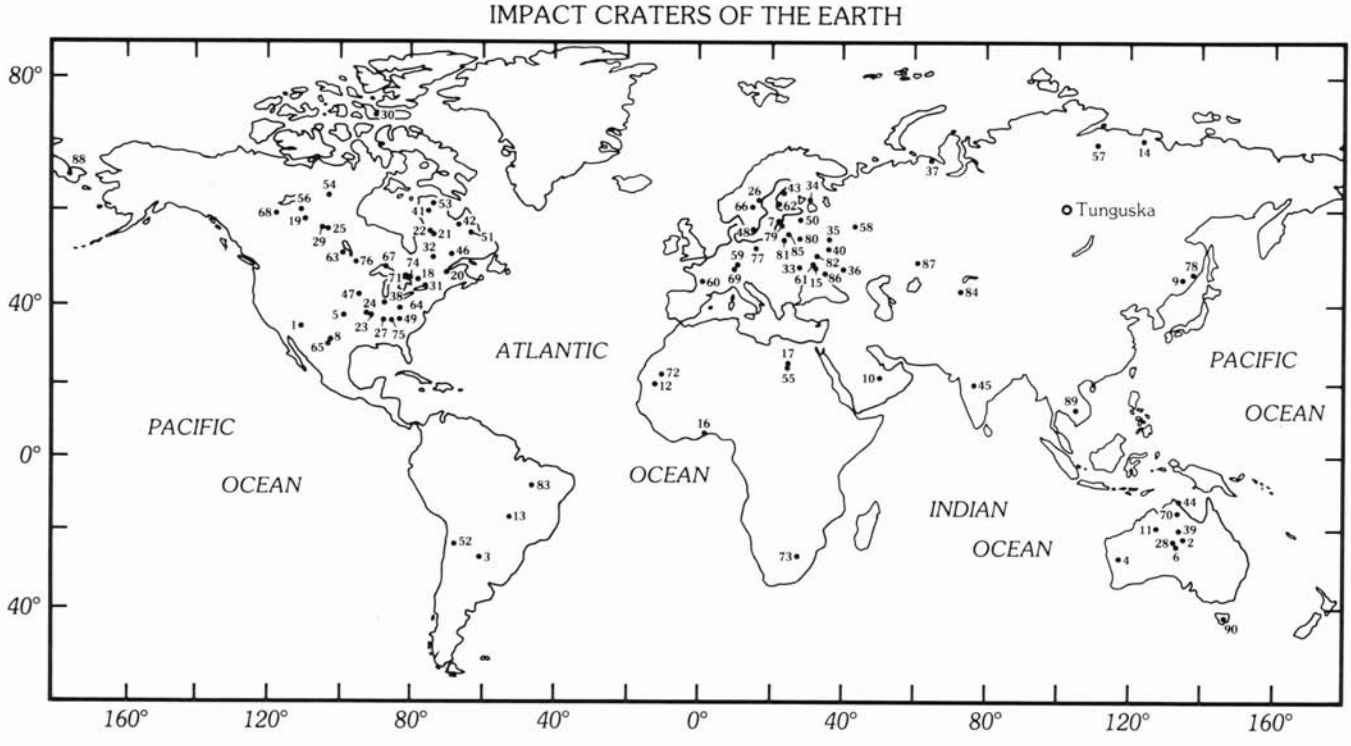

3.30 Distribution of presently known terrestrial impact structures.

There are 84 lunar craters with diameters greater than 161 km [110]. Ten classes may be distinguished, the oldest extending back to the time when saturation bombardment ceased. This date is given by Baldwin as 4.3 aeons (for an age of the Moon of 4.65 aeons!): 4.2 aeons seems to be a better estimate. This division into 10 classes may represent rather fine-tuning, and recognition of five classes may be more realistic [111].

The impact flux between 4.5 and 4.0 aeons is estimated to be 10^3–10^7 times the present flux rate [109]. The effect of this bombardment is to cause enormous rates of megaregolith production [112]. (The megaregolith in the highlands is estimated to be 2.5 km thick [113].) This cratering rate will cause very large amounts of mixing and overturning of crustal surfaces as well as destruction of thin crusts forming over magma oceans [112], and it is possible that we have generally underestimated these effects. "Pristine" lunar highland samples may be in fact very difficult to find. There does not seem to be any evidence in the cratering flux estimates that demands a spike at 3.8 aeons (Fig. 3.29), although this has frequently been suggested from the age and isotopic data (see next section). A preferred explanation is that ages are reset by the cratering events, so that the youngest events dominate. The similarity in surfaces exposed on the various planets and satellites lends credence to this view.

Estimates of the crater density versus age for the Moon, Earth, Mercury, Mars and Venus [108] are given in Fig. 3.31. Estimates of the relative ages of various geological provinces on Mercury and Mars from crater counting statistics are given in Tables 3.4 and 3.5.

3.17 The Cratering Record and the Lunar Cataclysm

Early intense cratering of the Moon was recognized long before the Apollo missions. The absence of landscapes on the Earth which resemble the

Table 3.4 Estimates of ages of geologic provinces on Mercury.†

Geologic Province	Crater Density Relative to Average Lunar Mare	Estimated Crater Retention Age (aeons)		
		Mimimum	Best Estimate	Maximum
Caloris Mare	3.7	2.4	3.8	4.0
Caloris whole basin	3.7	2.4	3.8	4.0
S. Polar uplands, intermediate diameter craters	5	3.0	3.9	4.0
S. Polar uplands, large diameter craters	20	4.1	4.4	4.5

†Adapted from *Basaltic Volcanism* (1981) Table 8.6.1.

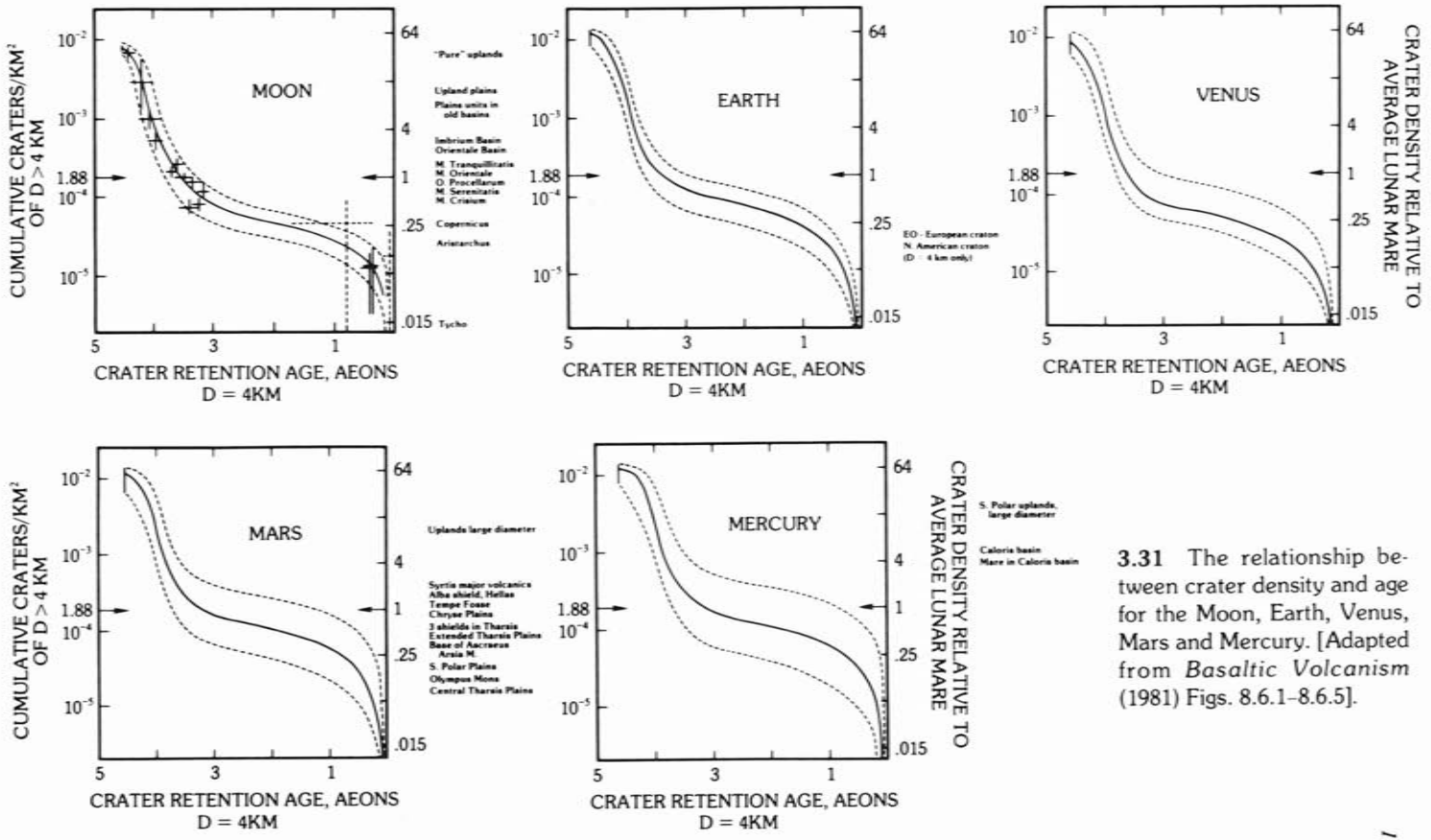

3.31 The relationship between crater density and age for the Moon, Earth, Venus, Mars and Mercury. [Adapted from *Basaltic Volcanism* (1981) Figs. 8.6.1–8.6.5].

Table 3.5 Estimates of ages of geologic provinces on Mars.[†]

Geologic Province	Crater Density · Relative to Average Lunar Mare	Estimated Crater Retention Age (aeons)			Map Symbol (Fig. 2.21)
		Minimum	Best Estimate	Maximum	
Central Tharsis volcanic plains	0.1	0.1	0.2	0.4	v
Olympus Mons volcano	0.15	0.1	0.3	0.7	v
Desert at bases of Ascraeus, Arsia Mons volcano	0.35	0.3	0.8	1.7	v
Extended Tharsis volcanic plains	0.49	0.6	1.2	2.7	v
Three shield volcanoes	0.63	0.8	1.7	3.2	v
Elysium volcanics	0.68	0.9	1.9	3.3	pv
Solis Planum volcanic plains	0.90	1.2	2.5	3.5	pm
Heavily cratered plains, small diameter craters	1.4	2.1	3.1	3.7	p
Chryse Planitia volcanic plain	1.4	2.1	3.1	3.7	p
Tyrrhena Patera volcanoes	1.4	2.1	3.1	3.7	pc
Heavily cratered plains, intermediate diameter craters	1.4	2.1	3.1	3.7	pc
Lunae Planum and Tempe Fossae cratered plains	1.5	2.4	3.3	3.8	pc
Syrtis Major Planitia volcanic plains	2.0	2.8	3.6	3.9	pc
Heavily cratered plains, large diameter craters	15	4.0	4.1	4.3	cu

[†]Adapted from *Basaltic Volcanism* (1981) Table 8.6.1.

lunar highlands indicated the likelihood that the intense bombardment preceded the exposed geological record, and may have been responsible for the destruction of a primitive crust. Estimates based on reasonable estimates of the cratering flux indicated that the mare surfaces were old [114]. Fielder [115] assumed a constant cratering flux throughout geological time, which gives ages for the maria of less than 700 million years. Hartmann [116] concluded that the early intense cratering rate was about 200 times that of the post-mare average rate and suggested an age of 3.5 billion years for the age of the mare flooding, essentially the correct age. He noted that "In a field so broad and intrinsically complex as planetary evolution, the application of Occam's razor to selected data is not necessarily the most direct way to correct conclusions." [116, p. 407].

A period of early intense cratering was immediately apparent from the Apollo 11 Preliminary Examination Team age data [117], which provided ages of 3–4 aeons for Mare Tranquillitatis. Since the relative stratigraphic sequence was already established, it was clear that the age of the heavily cratered highlands was about 4 aeons or older.

The relative age sequence of basins, as established by crater-counting and geological criteria, is vitally important for our understanding of the later stages of the great bombardment. Three versions are given in Table 3.1. Imbrium is widely recognized as the second youngest basin, with only Orientale being younger. Mare basalt ages of 3.8 aeons provide a younger limit, for their surfaces bear no trace of Imbrium or Orientale ejecta. The conventional date for Imbrium is 3.82 aeons (Section 5.2) taking the Fra Mauro ages at their face value. Orientale will be only slightly younger. The next question to be addressed is the relative ages of the Crisium, Serenitatis and Nectaris basins. Crisium is generally placed as the next oldest basin after Imbrium and probable secondaries from Crisium have been observed on Nectaris ejecta [90]. Serenitatis is probably dated at 3.86 aeons (Section 5.10). Earlier studies placed Serenitatis among the oldest of the near-side basins (Table 3.1). This apparent old age is interpreted as a result of heavy cratering of Serenitatis ejecta by Imbrium secondaries [90]. Accordingly, Serenitatis becomes one of the youngest of the lunar basins (Table 3.1), and it is no longer necessary to fit in several large basins, including Nectaris between Imbrium and Serenitatis. A currently unresolved question is whether Nectaris ejecta were sampled at the Apollo 16 site, the Descartes Formation being a possible candidate. The total number of Imbrian age basins is thus three, while Nectarian age basins number twelve and Pre-Nectarian basins number twenty-nine.

The cratering evidence does not suggest a spike, but rather a steady flux perhaps declining in the late stages of large objects striking the Moon (only three such craters occur post-Orientale), from Orientale back to the old nearly ruined basin of Al Khwarizmi (Fig. 3.32). The interpretation preferred here is that this flux increases backwards in time and that the earlier basins and

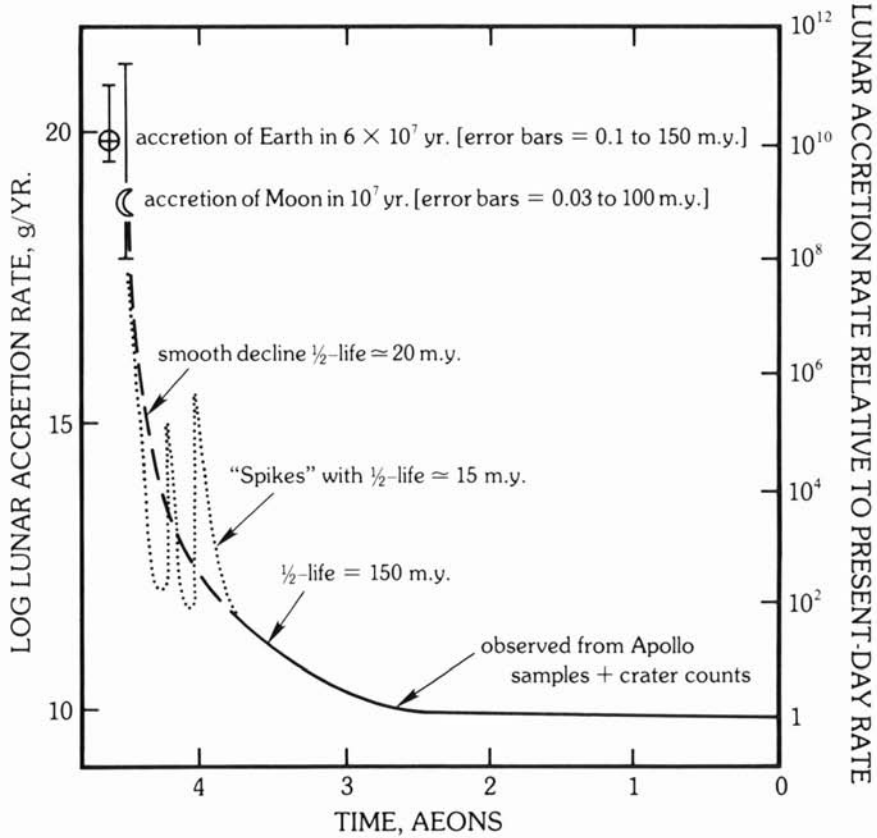

3.32 Schematic reconstruction of accretionary cratering without invoking a "spike" of catastrophic cratering 4 aeons ago. Present rate is observed (lower right) and projected back to 4 aeons ago using known impact rates determined from lunar dating. Additional datum is impact rate required to form Earth and Moon during their estimated formation intervals. Connection in "missing interval" from 4.5 to 4.0 aeons gives plausible planetesimal sweep-up half-lives of the order 20 to 45 m.y. [112]. (Courtesy W. K. Hartmann.)

craters have been obliterated. One predictable effect of a cataclysm should be the presence of many craters in the interval between the formation of Mare Imbrium and Mare Orientale. Baldwin [118] records only four 150-km-diameter craters. To these we may add the smaller Archimedes and Plato. This evidence does not suggest an intense spike in the flux rate, but is consistent with a uniform or declining flux of large impactors [119].

The relative age sequences of the old basins are thus critical for evaluation of the cataclysm concept. This has led to much polarization of opinion,

with one author labelling the cataclysm as a "misconception" or "myth" [120]. This topic is addressed again in Section 5.10, where the geochronological evidence from the lunar highland samples is assessed.

3.18 Secondary Cratering and the Cayley Problem

The problem of the relative volumes of primary and secondary ejecta produced by the multi-ring basin collisions is of primary importance for understanding much of lunar geology and geochemistry. This question is another facet of the Cayley problem and has been much debated, particularly in the context of the Apollo 16 samples. The basic question turns on whether the Cayley plains deposits are primary Imbrium ejecta or are reworked from local material by Imbrium secondaries. Relevant evidence comes from terrestrial studies.

At the Ries crater, the ejecta blanket out at two crater radii is 78% locally derived and has 22% primary crater ejecta (Fig. 3.24). The Ries example is particularly instructive, since the ejecta blanket crosses a geological boundary south of the crater, consisting of rock types not exposed at the crater site. Thus, the identification of local versus primary components in the ejecta blanket is simplified [60]. However, the problem is not so simply resolved on the Moon. In the absence of an atmosphere, most transport of material is by ballistic trajectory. In this context, there appears to be little evidence for turbulent flow in the well-exposed Hevelius Formation (Fig. 2.14). On the Moon, ejecta will travel further than on the Earth and with greater velocity. Hence, the ejected blocks possess considerable energy and will produce both secondary craters and extensive secondary ejecta.

The well-known landslide at the Apollo 17 site was probably triggered by Tycho ejecta impacting the top of the South Massif. It is suggested that this process is responsible for much of the valley filling in the highlands. That is, small impacts have transported highland materials into the depressions [121]. Thus, the similarity in chemistry between the surface samples on the Cayley Plains and the adjacent hilly Descartes Formation at Apollo 16 is explained. Certainly there is little difference in chemistry, age, or petrology.

Volumetric calculations tend to favor the secondary cratering hypothesis. Probably not enough ejecta can be derived from the basins to account for the widespread Cayley Formation. However, secondary craters excavate many times their own volume. About twice the original crater mass is deposited by the secondary craters out beyond the thick ejecta blankets [121].

This general explanation tying in the smooth plains to the great ringed basins solves some of the stratigraphic problems. Many lithologically similar units will be of different ages (Fig. 3.23), and much overlapping will occur. Major modifications will occur during the formation of the Orientale basin.

Some of the large post-mare craters may also contribute, as, for example, at the Apollo 17 landslide where the old highland material now overlies the younger mare lavas.

An observation in favor of the local derivation of much of the highland plains-forming units is that the geological mapping shows little relation to the orbital chemistry data [122]. Thus, there is no correlation between either the Al/Si values (as measured by the orbital XRF experiment) or with the orbital gamma-ray thorium values and the mapped distribution of Cayley Formation. For example, in areas showing high gamma-ray values, the amount of Cayley plains-type material may range from 0 to 85% [80]. This lack of correlation between chemistry and geology indicates that the plains-forming units do not originate as one uniform sheet of ejecta, but instead predominantly reflect the local geology, an argument for their local derivation.

This debate is likely to continue. Multi-ring basins are huge. If one formed in the present highland crust, it would excavate and distribute heterogeneous material. The obsession with the Cayley problem has overshadowed other aspects. Much primary basin ejecta also exists and perhaps dominates at the Fra Mauro site (Apollo 14), so providing a date for the Imbrium event. Even the Descartes Formation may be primary Imbrium ejecta piled up against the Kant Plateau, so negating our hopes of sampling primary Nectaris ejecta at the Apollo 16 site. Although the temperatures may be low and shock effects small in much of the ejecta, pods of melt and highly shocked material are probably present. These can provide for the thermal annealing in breccias, age resetting and the magnetic evidence of temperatures in excess of the Curie temperature of iron (750° C), at least locally.

References and Notes

1. Gilvarry, J. J. (1961) *Nature*. 190: 1048; Salisbury, J. W., and Ronca, L. B. (1966) *Nature*. 210: 669; Harrison, E. R. (1960) *Nature*. 188: 1064; Frey, H. (1977) *Icarus*. 32: 235; Green, D. H. (1972) *EPSL*. 15: 263.
2. Dana, T. D. (1846) *AJS*. 2: 235.
3. Spurr, J. E. (1944–49) *Geology Applied to Selenology*, Science Press, Lancaster, Pa.
4. Green, J. (1965) *Ann. N.Y. Acad. Sci.* 123: 385.
5. Fielder, G. (1967) *Lunar Geology*, Dufour, p. 162.
6. Moore, P., and Cattermole, P. J. (1967) *The Craters of the Moon*, Norton, N.Y., p. 10.
7. Gilbert, G. K. (1893) *Bull. Phil. Soc. Wash.* 12: 241.
8. Baldwin, R. B. (1949) *The Face of the Moon*, Univ. Chicago Press; (1963) *The Measure of the Moon*, Univ. Chicago Press.
9. Urey, H. C. (1952) *The Planets*, Yale Univ. Press; (1962) *Phys. Astron. Moon* (ed., A. Kopal), Academic Press N.Y., p. 484.
10. See review by Shoemaker, E. M. (1962) in *Phys. Astron. Moon* (ed., A. Kopal), Academic Press N.Y., p. 283.
11. Whitaker, E. A. (1974) NASA SP 330.

12. El-Baz, F., and Worden, A. M. (1972) NASA SP 289, 25-1.
13. Gault, D. E. (1966) in *Nature of the Lunar Surface*, John Hopkins Press, Baltimore, p. 135; (1964) in *The Lunar Surface Layer*, Academic Press, N.Y., p. 151.
14. See papers in *Shock Metamorphism of Natural Materials* (1968) (eds., French, B. M., and Short, M. N.), Mono Book Corp., Baltimore.
15. Baldwin, R. B. (1965) *A Fundamental Survey of the Moon*, McGraw Hill, N.Y., p. 137.
16. Von Bieberstein, M. (1802) *Untersuchungen über den Ursprung und die Ausbildung der gegenwartigen Anordnung des Weltgebaeudes*, Darmstadt; Gruithuisen, F. von P. (1829) *Analekten-Erd und Himmels-Kunde*, Munchen; see also [4].
17. Muehlberger, W. R., et al. (1980) *Lunar Highlands Crust*, p. 1.
18. Examples include the following works: Green, J. (1971) Copernicus as a lunar caldera, *JGR*. 76: 5719, Erlich, E. N., et al. (1974) General peculiarities of lunar volcanism, *Mod. Geol.* 5: 31; Leonardi, P. (1976) *Volcanoes and Impact Craters on the Moon and Mars*, Elsevier, 432 pp.; Miranova, M. N. (1970) NASA TT 566.
19. Pike, R. J. (1980) USGS Prof. Paper 1046-C.
20. Basic references are: *Impact and Explosion Cratering* (1977) (eds., Roddy, D. J., et al.), Pergamon Press, N.Y.; *Shock Metamorphism in Natural Materials* (1968) (eds., French, B. M., and Short, M. N.), Mono Book Corp., Baltimore.
21. Gault, D. E., et al. (1968) in *Shock Metamorphism of Natural Materials*, p. 87.
22. Dence, M. R., et al. (1977) in *Impact Cratering*, p. 247.
23. Grieve, R. A. F. (1977) in *Impact Cratering*, p. 791; (1980) *Lunar Highlands Crust*, p. 173.
24. Kieffer, S. W. (1977) in *Impact Cratering*, p. 751.
25. Kieffer, S. W., and Simonds, C. H. (1980) *Rev. Geophys. Space Phys.* 18: 143.
26. Oberbeck, V. R. (1977) in *Impact Cratering*, p. 45.
27. O'Keefe, J. D., and Ahrens, T. J. (1978) *PEPI.* 16: 341; (1981) *Rev. Geophys. Space Phys.* 19: 1.
28. Roddy, D. J. (1977) in *Impact Cratering*, p. 185.
29. Stöffler, D., et al. (1980) Multi-ring Basins Abstracts, 89.
30. Melosh, J. H. (1980) *Ann. Rev. Earth Planet Sci.* 8: 65.
31. Croft, S. K. (1980) *PLC 11*: 2347; (1981) *Multi-ring Basins*, p. 207, 227.
32. Fodor, R. V., and Taylor, G. J. (1979) *Impact*, Leisure Books, N.Y.
33. Roddy, D. J. (1978) *PLC 9*: 3891.
34. Pike, R. J. (1980) USGS Prof. Paper 1046-C. This comprehensive work should be consulted for a full and detailed discussion of lunar crater morphology.
35. Cintala, M. J., et al. (1977) *PLC 8*: 3409.
36. Dence, M. R., and Grieve, R. A. F. (1979) LPS X: 292; Dence, M. R., et al. (1977) *Impact Cratering*, p. 2470.
37. Pike, R. J. (1980) *Icarus*. 43:1; (1980) *PLC 11*: 2159.
38. Pohn, H. A., and Offield, T. W. (1970) USGS Prof. Paper 700-C, 153.
39. Settle, M., and Head, J. W. (1979) *JGR*. 84: 3081.
40. Settle, M. (1980) *Icarus*. 42: 1.
41. Gault, D. E., et al. (1975) *JGR*. 80: 2444.
42. Hale, W. S., and Head, J. W. (1979) *PLC 10*: 2623.
43. Milton, D. J., et al. (1972) *Science*. 175: 1199.
44. Wilshire, H. G., et al. (1973) USGS Prof. Paper 599-H, 42 pp.
45. Milton, D. J., and Roddy, D. J. (1972) IGC 24 Sec. 15, 119, Montreal.
46. Hale, W. S. (1980) *Lunar Highlands Crust*, p. 197. The megaregolith, of course, consists principally of basin deposits, with lesser amounts of crater ejecta. Accordingly,

layering is extensively developed, as for example, at Silver Spur at the Apollo 15 site (see Section 5.1.1).
47. Murray, J. B. (1980) *Moon and Planets*. 22: 269.
48. Maxwell, T. A. (1980) Multi-ring Basins Abstracts, 53.
49. Pieters, C., et al. (1981) LPS XII: 833.
50. Moore, H. J., et al. (1974) *PLC 5*: 71; McCauley, J. F. (1977) *PEPI*. 15: 220.
51. Head, J. W. (1974) *Moon*. 11: 327.
52. Baldwin, R. B. (1972) *PEPI*. 6: 327.
53. Hartmann, W. K., and Kuiper, G. (1962) *Comm. Univ. Ariz. Lunar Planet. Lab*. 1: 51.
54. Gault, D. E. (1971) *Lunar Geol. Primer*. 4: 137.
55. Hartmann, W. K., and Wood, C. A. (1971) *Moon*. 3: 3.
56. McCauley, J. F. (1977) *PEPI*. 15: 220.
57. Cadogan, P. H. (1974) *Nature*. 250: 315; Whitaker, E. A. (1981) *Multi-ring Basins*, p. 105.
58. Wilhelms, D. E., et al. (1977) *Impact Cratering*, p. 539.
59. Dence, M. R. (1976) LS V: 165.
60. Hörz, F., and Banholzer, G. S. (1980) *Lunar Highlands Crust*, p. 211.
61. Whitford-Stark, J. L. (1981) *Multi-ring Basins,* p. 113.
62. Hodges, C. A., and Wilhelms, D. E. (1978) *Icarus*. 34: 294.
63. Hartmann, W. K., and Wood, C. A. (1977) *Moon*. 3: 3.
64. Roddy, D. J. (1976) *PLC 7*: 3027.
65. Roddy, D. J. (1977) *Impact Cratering*, p. 185.
66. Grieve, R. A. F. (1980) *Lunar Highlands Crust*, p. 173; Dence, M. R., and Grieve, R. A. F. (1979) LPS X: 292.
67. Wood, C. A., and Gifford, A. W. (1980) Multi-ring Basins Abstracts, 121.
68. Hartmann, W. K., and Kuiper, G. P. (1962) *Comm. Univ. Ariz. Lunar Planet. Lab*. 1: 51.
69. Wollenhaupt, W. R., et al. (1973) NASA SP 330, p. 33.
70. Cadogan, P. H. (1976) *Nature*. 250: 315. See also Hartmann, W. K., and Wood, C. A. (1971) *Moon*. 3: 4; Hodges, C. A., and Wilhelms, D. E. (1978) *Icarus*. 34: 294.
71. Hale, W. S., et al. (1980) Multi-ring Basins Abstracts, 30.
72. Trask, N. J., and Guest, J. E. (1975) *JGR*. 80: 2461.
73. Head, J. W., et al. (1975) *PLC 6*: 2805.
74. Herzberg, C. T., and Baker, M. B. (1980) *Lunar Highlands Crust*, p. 113.
75. Hawke, B. R., and Head, J. W. (1978) LPS IX: 477.
76. Wood, C. A., and Head, J. W. (1976) *PLC 7*: 3629.
77. Wood, C. A. (1980) *PLC 11*: 2221.
78. Grieve, R. A. F., and Robertson, P. B. (1979) *Icarus*. 38: 212.
79. Wood, C. A., et al. (1978) *PLC 9*: 3691.
80. Cintala, M. J., et al. (1977) *PLC 8*: 3409.
81. Hawke, B. R., and Head, J. W. (1977) *Impact Cratering*, p. 815.
82. Mendell, W. W. (1976) *PLC 7*: 2705.
83. Oberbeck, V. R., and Morrison, R. H. (1973) *PLC 4*: 107.
84. Schultz, P. A. (1976) *Moon Morphology*, Univ. Texas Press, Austin.
85. Schultz, P. H., and Singer, J. (1980) *PLC 11*: 2243.
86. Greeley, R., et al. (1977) *JGR*. 82: 8011.
87. Batson, R. M., et al. (1979) *Atlas of Mars*, NASA SP-48, 146 pp.
88. Greeley, R., et al. (1980) *PLC 11*: 2075.
89. Gault, D. E., et al. (1975) *JGR*. 80: 2444.
90. Wilhelms, D. E. (1976) *PLC 7*: 2883.

91. Escape velocities for Mimas are 0.16 km/sec, for Dione, 0.50 km/sec and for Rhea, 0.65 km/sec.
92. Shoemaker, E. M., and Wolfe, R. F. (1981) LPS XIIA: 1.
93. Head, J. W., and Wilson, L. (1979) *PLC 10*: 2861.
94. Although not strictly analogous, it is of interest to recall the Revelstoke event, where black CCl powder was recovered from a frozen lake surface [Folinsbee, R. E., et al. (1967) *GCA*. 31: 1625].
95. Hawke, B. R., and Bell, J. F. (1981) LPS XII: 412.
96. Schultz, P. H. (1976) *Moon*. 15: 241; Pike, R. J. (1971) *Icarus*. 15: 384.
97. Hall, J. L., et al. (1981) *JGR*. 86: 9537. This paper provides the most recent discussion on mechanisms for forming floor fractured craters.
98. Dvorak, J., and Phillips, R. J. (1978) *PLC 9*: 3651.
99. Dvorak, J., and Phillips, R. J. (1977) *GRL*. 4: 380.
100. El-Baz, F. (1972) NASA SP-315, p. 29–93.
101. Evans, R. E., and El-Baz, F. (1973) LS IV: 231.
102. Schultz, P., and Srnka, L. J. (1980) *Nature*. 284: 22.
103. Hood, L. L., et al. (1979) *Science*. 204: 53.
104. Grieve, R. A. F., and Dence, M. R. (1979) *Icarus*. 38: 230.
105. Hartmann, W. K. (1965) *Icarus*. 4: 157.
106. Palme, H., et al. (1978) *GCA*. 42: 313.
107. Grieve, R. A. F., and Robertson, P. B. (1979) *Icarus*. 38: 212.
108. *Basaltic Volcanism* (1981) Section 8.6.
109. Lange, M. A., and Ahrens, T. J. (1979) *PLC 10*: 2707.
110. Baldwin, R. B. (1981) *Multi-ring Basins*, p. 275.
111. Wilhelms, D. E., pers. comm., 1981.
112. Hartmann, W. K. (1980) *Lunar Highlands Crust*, p. 155.
113. Head, J. W. (1976) *PLC 7*: 2913.
114. Kuiper, G. P. (1954) *Proc. Nat. Acad. Sci*. 40: 1104; Urey, H. C. (1952) *The Planets*, Yale; (1960) *Astrophys. J*. 132: 502.
115. Fielder, G. (1963) *Nature*. 198: 1256.
116. Hartmann, W. K. (1965) *Icarus*. 4: 207; (1966) *Icarus*. 5: 406.
117. LSPET (1969) *Science*. 165: 1211.
118. Baldwin, R. B. (1974) *Icarus*. 23: 97.
119. Wetherill, G. W. (1981) LPS XII: 1176; (1981) *Multi-ring Basins*, p. 1.
120. Hartmann, W. K. (1975) *Icarus*. 24: 181.
121. Oberbeck, V. R., et al. (1973) NASA Tech. Memo. TMX 62302. 54 pp.
122. Hörz, F., et al. (1974) LS V: 357.